Interactions and dynamics in Li + Li_2 ultracold collisions

Marko T. Cvitaš*, Pavel Soldán†, and Jeremy M. Hutson
Department of Chemistry, University of Durham, South Road, Durham, DH1 3LE, UK

Pascal Honvault‡ and Jean-Michel Launay
UMR 6627 du CNRS, Laboratoire de Physique des Atomes, Lasers, Molécules et Surfaces, Université de Rennes, 35042 Rennes Cedex, France

A potential energy surface for the lowest quartet electronic state ($^4A'$) of lithium trimer is developed and used to study spin-polarized Li + Li_2 collisions at ultralow kinetic energies. The potential energy surface allows barrierless atom exchange reactions. Elastic and inelastic cross sections are calculated for collisions involving a variety of rovibrational states of Li_2. Inelastic collisions are responsible for trap loss in molecule production experiments. Isotope effects and the sensitivity of the results to details of the potential energy surface are investigated. It is found that for vibrationally excited states the cross sections are only quite weakly dependent on details of the potential energy surface.

PACS numbers: 34.20.-b,34.20.Mq,34.50.Ez,34.50.-s,82.20.Ej,82.20.Kh

I. INTRODUCTION

There is great interest in the properties of molecules formed in laser-cooled atomic gases by processes such as photoassociation and magnetic association.[1,2,3] Diatomic molecules have been formed from bosonic and/or fermionic species of all the alkali metals from Li to Cs. Dimers of bosonic species have usually been found to decay quickly because of inelastic collisions with other atoms,[4,5,6,7] but for fermionic species (^{6}Li, ^{40}K) it has been possible to stabilise the dimers by tuning to large positive values of the atom-atom scattering length.[8,9,10] This approach was used in late 2003 to create long-lived Bose-Einstein condensates of fermion dimers,[11,12,13] and since that time there has been a large amount of work on their properties, and particularly on the transition between Bose-Einstein condensation (BEC) and the Bardeen-Cooper-Schrieffer (BCS) regime characterised by long-range Cooper pairing and superfluidity.

Photoassociation and magnetic association (tuning through zero-energy Feshbach resonances) both produce molecules that are initially in very highly excited vibrational states. However, there is great interest in bringing these molecules down to low vibrational states and ultimately to the absolute ground state. For example, Staanum *et al.*[14] have produced Cs_2 in vibrational levels $v = 4$ to 6 of the $a^3\Sigma^+$ state and studied collision processes, while Sage *et al.*[15] have produced small numbers of ultracold polar RbCs molecules in their absolute ground state by a 4-photon process.

*Present address: University Chemical Laboratory, Lensfield Road, Cambridge, CB2 1EW, UK
†Present address: Doppler Institute, Department of Physics, Faculty of Nuclear Sciences and Physical Engineering, Czech Technical University, Břehová 7, 115 19 Praha 1, Czech Republic
‡Present address: Institut UTINAM, UMR CNRS 6213, Université de Franche-Comté, 25030 Besançon Cedex, France

Ultracold molecules are initially formed in the presence of ultracold atoms and can collide with them.[16] For molecules in vibrationally excited states, there is the possibility of vibrationally inelastic collisions,

$$M_2(v) + M \longrightarrow M_2(v' < v) + M, \qquad (1)$$

where v is the vibrational quantum number. Since the trap depth is usually much less than 1 K, such collisions always release enough kinetic energy to eject both collision partners from the trap. If the molecular density is high, there is also the possibility of inelastic molecule-molecule collisions,

$$M_2(v) + M_2(v) \longrightarrow M_2(v' < v) + M_2(v'' \leq v). \qquad (2)$$

Molecules are not *destroyed* in inelastic collisions, but they are lost from the trap and are no longer ultracold.

The rates of inelastic atom-molecule collisions involving alkali metal dimers have been studied both experimentally[14,17,18,19] and theoretically.[20,21,22,23,24,25,26] Wynar *et al.*[17] formed $^{87}Rb_2$ molecules in the second-to-last vibrational level of the ground excited state by stimulated Raman adiabatic passage (STIRAP). They estimated an upper bound of $k_{\rm loss} = 8 \times 10^{-11}$ cm^3 s^{-1} due to inelastic atom-molecule collisions. Mukaiyama *et al.*[18] measured the trap loss rate for $^{23}Na_2$ molecules formed by Feshbach resonance tuning and obtained an atom-molecule rate coefficient $k_{\rm loss} = 5.1 \times 10^{-11}$ cm^3 s^{-1} for molecules in the highest vibrational state. Staanum *et al.*[14] investigated inelastic collisions of rovibrationally excited Cs_2 ($^3\Sigma_u^+$) in collisions with Cs atoms in two different ranges of the vibrational quantum number v by monitoring trap loss of Cs_2. They obtained atom-molecule rate coefficients close to 1.0×10^{-10} cm^3 s^{-1} for both $v = 4$ to 6 and $v = 32$ to 47. Zahzam *et al.*[19] carried out similar work for different rovibrational states of $^3\Sigma_u^+$, and also considered molecules in the $^1\Sigma_g^+$ state and molecule-molecule collisions. They obtained rate coefficients of 2.6×10^{-11}

$cm^3\ s^{-1}$ and 1.0×10^{-11} $cm^3\ s^{-1}$ in the atom-atom and atom-molecule cases respectively, both with quite large error bounds.

Quantum dynamics calculations on alkali metal atom–diatom collisions were first carried out by Soldán *et al.*,[20] using the potential energy surface of Higgins *et al.*[27] and subsequently extended to K + K_2 on a new potential surface.[24] In parallel work, Petrov *et al.*[22,23] analysed the stability of fermion dimers in terms of the long-range form of the wavefunction. In the case where the atom-atom scattering length a is much larger than the range of the atom-atom potential r_e, they showed that both atom-molecule and molecule-molecule inelastic collision rates are suppressed by Fermi statistics. However, their derivation applies only to molecules that are in long-range states, with a wavefunction that depends on the atom-atom scattering length a, with $\chi(r) \sim \exp(-r/a)$. In the present paper, we show computationally that there is *no* systematic suppression of the atom-molecule inelastic rate for ^{6}Li dimers in low-lying vibrational levels, even when a is large and positive. We also consider mixed-isotope Li + Li_2 collisions. This has been reported briefly in previous work,[25,26] but the present paper gives full details of the calculations and further details of the results.

The structure of the paper is as follows. Section II describes calculations of the potential energy surface for quartet Li_3, including details of both the electronic structure methods employed and the procedures used to interpolate between and extrapolate beyond the *ab initio* points. The surface allows barrierless atom exchange reactions. Section III describes atom + diatom reactive scattering calculations both for homonuclear systems [bosonic, ^{7}Li + $^7Li_2$ and fermionic, ^{6}Li + $^6Li_2$] and mixed-isotope systems. For collisions of ^{7}Li with either $^6Li_2$ or ^{6}Li^{7}Li, exoergic atom exchange reactions are possible even for ground-state molecules because of the differences in zero-point energies. Section III also explores the sensitivity of the cross sections to the potential energy surface and shows that for vibrationally excited states the dependence is relatively weak (only a factor of 2 for molecules initially in $v = 3$). Section IV presents conclusions and prospects for future work.

II. QUARTET POTENTIAL ENERGY SURFACES FOR Li_3

In previous work, we investigated nonadditive forces in spin-polarized (quartet) alkali metal trimers[28] at linear and equilateral geometries. For Li_3, we found very large nonadditive forces at equilateral geometries that reduced the interatomic distance by more than 1 Å and increased the well depth by a factor of 4 with respect to the sum of Li–Li pair potentials. We subsequently gave a brief description of the complete potential energy surface[25] and identified a seam of conical intersections at collinear geometries between $^4\Sigma$ and $^4\Pi$ states. The conical intersection has been investigated further by Brue *et al.*[29] The seam results in a cusp at energies close to the atom-diatom threshold and influences Li + Li_2 collision dynamics at ultralow energies.[25,26] In the present paper, we give a full description of the *ab initio* calculations and fitting procedure used to obtain a global representation of the surface and extend the collision calculations.

A. Electronic states overview

In the present work, we are interested mostly in the lowest quartet electronic state of Li_3, which is a $^4A'$ state in C_s symmetry. This state correlates with three ground-state (^2S) atoms at large interatomic separations. As mentioned above, the quartet ground state has crossings with other electronic states that correlate with the $S + S + P$ separated-atom limit. These crossings (and avoided crossings) occur at energies that are potentially relevant to scattering processes involving three ground-state Li atoms. To gain a broader, qualitative picture on how the different potential energy surfaces intertwine, we have carried out state-averaged multiconfiguration self-consistent field (MCSCF) calculations of the potential energy surfaces of quartet states for certain high-symmetry arrangements. These calculations used the complete active space (CASSCF) method of Werner and Knowles,[30,31,32,33,34] as implemented in the MOLPRO package,[35] with an aug-cc-pVTZ basis set generated from the cc-pVTZ set[36] as described below. The active space included all 24 molecular orbitals constructed principally from 2s, 2p, 3s and 3p atomic orbitals, with the three 1s orbitals doubly occupied in all configurations; this active space is designated [3,24] below.

Figure 1 shows the potential curves obtained for quartet states at $D_{\infty h}$ geometries. The ground state is of Σ_u symmetry; at a Li-Li bond length r near 3 Å it intersects a Π_g state, which in turn intersects a Σ_g state at higher energies. If we change the interbond angle α, keeping the two adjacent bond lengths unchanged (moving from $D_{\infty h}$ to C_{2v} arrangements), the ground state becomes of B_2 symmetry, while the Π_g state splits into states of A_2 and B_2 symmetries. The two B_2 states avoided-cross around $\alpha = 70°$. At D_{3h} arrangements ($\alpha = 60°$), shown in Figure 2, the ground state is of A_2' symmetry, while the second B_2 state forms a doubly degenerate E' state with the A_1 state that originated from Σ_g at $D_{\infty h}$. The A_2 state in C_{2v} symmetry ($\Pi_g = A_2 + B_2$) forms an E'' state with the B_1 state that was a part of $\Pi_u = A_1 + B_1$ at $D_{\infty h}$.

For comparison, Figure 3 shows the triplet states of Li_2 calculated using [2,8]-CASSCF, followed by an internally contracted multireference configuration interaction (MRCI)[34,37,38,39] including single and double excitations from the CASSCF wavefunction.

Figure 4 shows a correlation diagram that connects the $D_{\infty h}$, D_{3h} and atom-diatom (C_{2v}) limits for states of quartet Li_3 that correlate with the $S + S + P$ atomic limit for fixed bond length of 6 Å. Note that the molecular

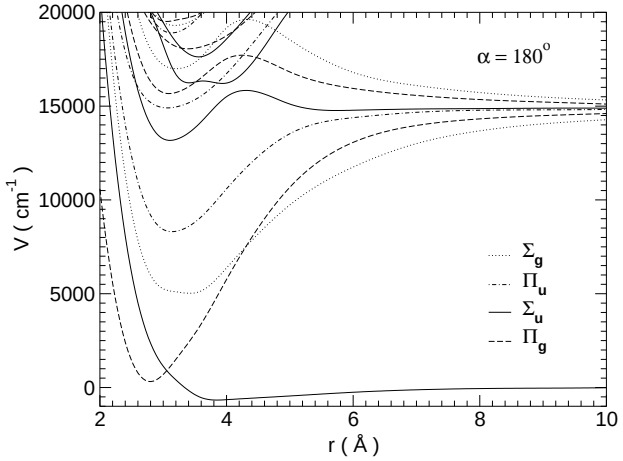

FIG. 1: CASSCF quartet potentials of Li_3 at $D_{\infty h}$ geometries for states that correlate with the atomic S+S+S and S+S+P asymptotic limits. The interatomic distances are r, r, and $2r$.

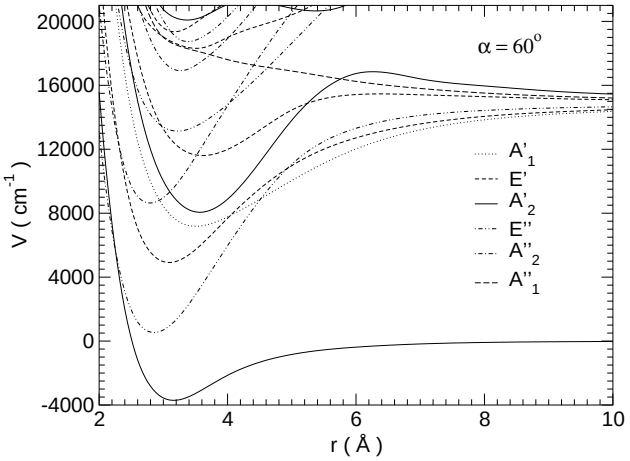

FIG. 2: CASSCF quartet potentials of Li_3 at D_{3h} geometries for states that correlate with the atomic S+S+S and S+S+P asymptotic limits. The interatomic distances are r.

state arising from three S-state atoms is not shown.

In the present work we focus on calculating the lowest quartet state, $^4A'$, to high precision. Colavecchia *et al.*[40] and Brue *et al.*[29] have carried out full configuration interaction (FCI) calculations with just one electron on each Li atom correlated. Our calculations differ from theirs in correlating all electrons and in using considerably larger basis sets, but use approximate correlation treatments.

B. Basis set convergence

A variety of basis sets are available for lithium. Feller[36] constructed correlation-consistent polarized valence basis sets (cc-pVXZ for X=D, T, Q, and 5)[41] and Iron *et al.*[42] devised correlation-consistent polarized core-valence

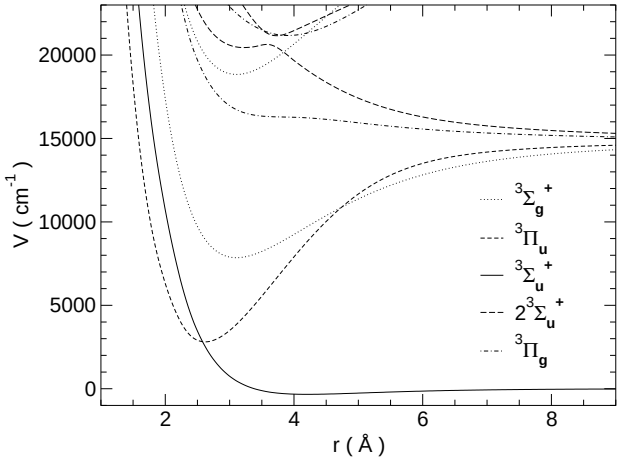

FIG. 3: Triplet potential energy curves of Li_2 from the atomic $S + S$ and $S + P$ dissociation limits.

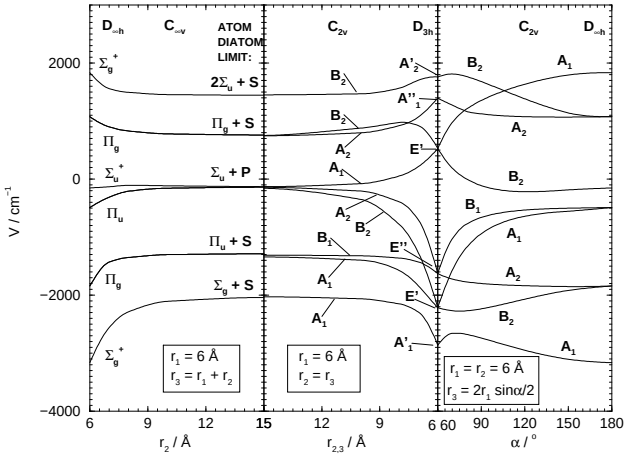

FIG. 4: Correlation diagram of quartet potentials of Li_3 that correlate with the atomic $S + S + P$ dissociation limit. Note the the energy is shown relative to this limit and the state correlating with $S + S + S$ is not shown. The first panel connects the $D_{\infty h}$ states with the atom-diatom limit, with one interatomic distance fixed at 6 Å and $C_{\infty v}$ symmetry preserved. The second panel connects the atom-diatom limit with D_{3h} states, with one interatomic distance fixed at 6 Å and C_{2v} symmetry preserved. The third panel connects D_{3h} and $D_{\infty h}$ terms, with two interatomic distances fixed at 6 Å and the angle between them, α, varied.

basis sets (cc-pCVXZ) by adding "tight" functions to Dunning-type cc-pVXZ bases in order to give a better account of the core-core and core-valence correlation. There are no standard augmented basis sets available for Li,[36] so we generated augmented variants of several basis sets using the even-tempered scheme implemented in MOLPRO, which adds an additional diffuse function of each angular symmetry (s, p, d, f, ...), with an even-tempered exponent based on the ratio of the two smallest exponents in the original set (or a ratio of 2.5 if only one

function of a type is present in the original basis).

The cc-pVXZ and cc-pCVXZ basis sets are usually used with the s and p functions contracted. However, in previous work on alkali metal trimers,[28] we found it advantageous to use the basis sets in uncontracted form. In the present work we consider the cc-pV5Z basis set in three different forms: fully contracted (sp-contracted), fully uncontracted, and with just the p space uncontracted (s-contracted). However, we found it too expensive to uncontract the cc-pCVXZ and augmented basis sets and these were used in fully contracted form.

We chose to use RCCSD(T) calculations (restricted open-shell coupled cluster with single, double and noniterative triple excitations). All calculations were carried out using MOLPRO.[35]

With the computer resources available to us, we found that RCCSD(T) calculations of triatomic energies with the largest basis sets available, cc-pCV5Z and aug-cc-pCV5Z, were feasible only for relatively small numbers of points, not for a grid of several hundred points. These basis sets were therefore used only for atomic and diatomic calculations, except that the cc-pCV5Z basis set was used to provide benchmark triatomic calculations at a restricted number of points.

We began by testing convergence of two atomic properties, the static polarizability and the S–P excitation energy, which are important for accurate calculations of long-range forces. The results for a variety of basis are shown in Table I. In general terms all the basis sets perform acceptably for both quantities, though the s-contracted cc-pV5Z basis set is fortuitously accurate for the S–P excitation energy.

We next considered the performance of different basis sets on potential curves for the $^3\Sigma_u^+$ state of Li_2. Electronic energies were calculated on a mesh of 64 interatomic distances. The results were corrected for basis-set superposition error (BSSE) using the counterpoise correction.[46] The points were then interpolated using the reciprocal power reproducing kernel Hilbert space (RP-RKHS) interpolation method[47,48] with dispersion coefficients C_6, C_8 and C_{10} fixed to accurate values from the calculations of Yan *et al.*[49] At internuclear distances $r > 16$ Å the *ab initio* energies were replaced by those from the three-term dispersion formula. Other interpolation parameters, in the notation of Ref. 48, were $m = 2$, $n = 3$, $r_a = 15$ Å, $r_{65} = 21.5$ Å, $r_{66} = 22.5$ Å, $r_{67} = 23.5$ Å.

The resulting diatomic well depth D_e and bond length r_e are included in Table I, together with the binding energy of the last bound state E_{10} and scattering length a calculated for $^7Li_2$. The results are compared with properties obtained from the RKR curves of Linton *et al.*[50] (the values of a and E_{10} are from photoassociation spectroscopy in combination with RKR results[51]). It may be seen that all the basis sets underestimate the RKR well depth by between 2 and 5 cm^{-1}, except for the cc-pCVQZ basis set which underestimates it by 8 cm^{-1} and the sp-contracted cc-pV5Z basis set which slightly overestimates it. On this basis we excluded the cc-pCVQZ basis set from further consideration.

Another way to test the quality of a basis set is to consider the magnitude of BSSE. BSSE arises when basis functions on two centers overlap and compensate for inadequacies in the one-centre basis. Table I shows dimer BSSE values at $r = 4.2$ Å, which is near the potential minimum. The cc-pCVXZ basis sets give quite small BSSE values since they are by construction geared to represent the core-core correlation well. However, as discussed above, the cc-pCVQZ basis set is not accurate enough for our purposes and the cc-pCV5Z basis set is too expensive. We therefore focussed on the cc-pV5Z basis sets. As may be seen in Table I, the cc-pV5Z basis set in sp-contracted form gives a very large BSSE, 41.45 cm^{-1} at $r = 4.2$ Å, which we considered unacceptably high. However, uncontracting the p space reduces this to 2.553 cm^{-1}. Uncontracting the s space as well reduces this by a further factor of 3, but at a very considerable computational cost.

Finally, we carried out convergence tests on triatomic energies. In this case there are no experimental results to compare with, so we used the position and energy of the equilateral minimum, calculated with the cc-pCV5Z basis set, as our benchmark. As may be seen in Table I, there is very little difference between the s-contracted and uncontracted forms of the cc-pV5Z basis set, which underestimate the cc-pCV5Z well depth by 11 and 13 cm^{-1} respectively. However, the sp-contracted form overestimates the well depth by 40 cm^{-1}. For triatomic RCCSD(T) calculations the s-contracted basis set costs only 10% more than the sp-contracted set, which the fully uncontracted set costs twice as much. On this basis we decided to proceed with the s-contracted cc-pV5Z basis set to calculate the full potential surface.

One further possibility we considered was the use of frozen-core calculations, which are considerably cheaper than calculations that correlate all electrons. However, we found that such calculations systematically overestimate dimer well depths by 2 to 3% and equilibrium distances by about 2% compared to cc-pCVXZ calculations at each level (T, Q, Z). For example, frozen-core calculations with the sp-contracted cc-pV5Z basis set give $D_e = 338.471$ cm^{-1} and $r_e = 4.199$ Å for Li_2. Frozen-core calculations on the trimer with this basis set *underestimate* the trimer well depth, giving $D_e = 3937.5$ cm^{-1} and $r_e = 3.137$ Å. We therefore did not pursue the frozen-core approximation.

As described above, the Li_3 potential shows a seam of conical intersections at linear geometries. The RCCSD(T) approach is inherently a single-reference method, so its appropriateness in the vicinity of a conical intersection is open to question. The usual approach is to consider the T1 diagnostic, which can be used to identify where multireference effects become large and may compromise the results. Lee and Taylor[52] have given a rule of thumb that single-reference methods become unreliable when T1 > 0.02. In the present calculations, the T1 diag-

basis set	Atomic	Diatomic					Triatomic		
	$\alpha(a_0^3)$	S–P energy (cm^{-1})	r_e (Å)	D_e (cm^{-1})	a (a_0)	E_{10} (cm^{-1})	BSSE (cm^{-1})	r_e (Å)	D_e (cm^{-1})
sp-contracted cc-pV5Z	165.518	14834.01	4.169	334.042			41.45	3.102	4021.5
s-contracted cc-pV5Z	164.396	14903.62	4.177	328.922	12.54	0.223	2.553	3.102	3969.8
uncontracted cc-pV5Z	164.336	14906.69	4.177	328.732			0.8015	3.102	3967.4
aug-cc-pCV5Z	164.189		4.176	330.548	−8.95	0.346	0.234		
cc-pCV5Z	164.152	14906.48	4.175	328.952			0.139	3.098	3980.6
cc-pCVQZ	164.140	14911.28	4.179	325.499			0.501		
Best available theory	164.111[a]								
Experiment	164.0±3.4[b]	14903.89[c]	4.173	333.69	-27.3 ± 0.8	0.416			

TABLE I: Convergence tests for Li basis sets. For atoms: static polarizability α and S–P excitation energy. For triplet dimers: dissociation energy D_e, position of the minimum r_e, BSSE evaluated at $r = 4.2$ Å scattering length a and energy of the highest vibrational level E_{10} for the $^7Li_2$ molecule. For quartet trimers, dissociation energy D_e and position of the minimum r_e for Li_3 (D_{3h}). All calculations except "best available theory" are from the present work and used RCCSD(T) calculations. [a]: ref. 43; [b]: ref. 44; [c]: ref. 45.

nostic was relatively small at near-linear geometries but had a maximum value of around 0.11 at equilateral geometries. We therefore investigated the reliability of the RCCSD(T) approach by recalculated the Li_3 potential energy surface with a smaller basis set (aug-cc-pVTZ), using [3,12]-CASSCF followed by a multireference configuration interaction (MRCI) calculation including Davidson's correction, and compared it with the corresponding RCCSD(T) energies. The T1 diagnostic was again large in the well region for bond angles of $\sim 60°$. Nevertheless, the two surfaces agreed within 2% in well depth with no visible qualitative differences. We therefore believe that the RCCSD(T) energies obtained with the cc-pV5Z basis set are trustworthy.

C. The $1^4A'$ surface

1. Representation of the surface

If the potential is to be capable of representing all the properties of experimental interest (including atom-atom scattering lengths, dimer and trimer bound states, atom-diatom collisions and 3-body recombination), then it is very important that it should represent dissociation into all possible sets of products (atom + diatom and 3 separated atoms) with the correct long-range behaviour. In our previous work on K + K_2,[24] this was achieved by separating the potential into pairwise-additive and non-additive parts and interpolating them separately,

$$V(\mathbf{r}) = \sum_{i<j}^{3} V_{\mathrm{dimer}}(r_{ij}) + V_3(\mathbf{r}), \qquad (3)$$

where $\mathbf{r}$ represents (r_{12}, r_{23}, r_{31}) and the functional form for the nonadditive part $V_3(\mathbf{r})$ is chosen to ensure the correct behaviour in the atom-diatom limit.[53] However, for Li + Li_2 the non-additive term is so large that the potential minimum for the trimer occurs at a distance that is high on the repulsive wall for the dimer. Because of this, Eq. (3) would represent the interaction potential in this region as a difference between two very large quantities. This is unsatisfactory. Nevertheless, at long range a decomposition according to Eq. (3) is essential. Under these circumstances, it is best to fit the *ab initio* points directly to obtain a short-range function $V_{\mathrm{SR}}(\mathbf{r})$ without imposing the correct long-range behaviour, and to join this onto a potential with the proper long-range behaviour $V_{\mathrm{LR}}(\mathbf{r})$ using a switching function $S(\mathbf{r})$,

$$V(\mathbf{r}) = S(\mathbf{r})V_{\mathrm{SR}}(\mathbf{r}) + [1 - S(\mathbf{r})]V_{\mathrm{LR}}(\mathbf{r}). \qquad (4)$$

The switching function is 1 at short range but switches smoothly to zero at long range as described below.

2. Choice of grid

For quantum dynamics calculations, it is very important to represent the potential energy function smoothly and without oscillations between *ab initio* points. There are several coordinate systems that can be used for triatomic systems, including hyperspherical coordinates, Jacobi coordinates, valence (bond length / bond angle) coordinates and pure bond-length coordinates. These are by no means equivalent for interpolation purposes. As will be seen below, the dynamical calculations are carried out in hyperspherical coordinates. However, grids of points in hyperspherical coordinates tend to include points in which 2 atoms lie very close together, which hinders interpolation because polynomials with very high localised maxima tend to have oscillations in other regions. Jacobi coordinates suffer from the same problem, and neither Jacobi coordinates nor valence coordinates allow the full 3-body exchange symmetry to be introduced in a natural way. Fortunately, there is no need to represent the potential energy surface in the same coordinate system as is used in the dynamical calculations. We

therefore chose to carry out electronic structure calculations on a grid of points in pure bond-length coordinates (r_{12}, r_{23}, r_{31}), which make exchange symmetry easy to handle but avoid points with atoms too close together.

The grid was constructed using the internuclear distances r = 2.0, 2.4, 2.8, 3.2, 3.6, 4.0, 4.4, 4.8, 5.2, 6.0, 6.8, 8.4 and 10.0 Å. At nonlinear geometries, the grid included all 315 unique combinations of (r_{12}, r_{23} and r_{31}) taken from this set that satisfy the triangle inequality, $r_{31} < r_{12} + r_{23}$. We also added additional points for which r_{12} and r_{23} are in this set and r_{31} takes values larger than 10.0 Å in steps of 1.6 Å. This produced another 56 points, such as, for example, (6.0, 6.0, 11.6) Å. A grid of 120 linear configurations ($r_{31} = r_{12} + r_{23}$) was formed by taking all possible combinations of r_{12} and r_{23} from the above set with the additional distance 5.6 Å. We calculated electronic energies at a total of 491 geometries.

Interaction energies for the $^4A'$ state were calculated with respect to the 3-atom $S + S + S$ dissociation limit using RCCSD(T) calculations with the s-contracted cc-pV5Z basis set described above. All interaction energies were corrected for BSSE using the counterpoise correction.[46]

3. Fitting and interpolation

Even with almost 500 points, the grid is fairly sparse and the quality of interpolation is important. However, many interpolation procedures in N dimensions work only for a "product" grid, in which points are available at all combinations of a set of coordinate values. This cannot be provided in pure bond length coordinates because of the need to satisfy the triangle condition. We therefore chose to use the interpolant-moving least squares (IMLS) method.[54] In this approach, approximate gradients and Hessians are calculated at each grid point and stored. The fitting function is represented as a weighted sum of Taylor expansions of second order about the grid points.

The IMLS procedure has two parameters, the power p that determines the shape and range of the weight function and a smoothing parameter ϵ that removes the flat spots at data points. Figure 5 shows IMLS fits to the potential for $D_{\infty h}$ geometries in the region of the conical intersection, with $p = 6$ and ϵ values of 0.03 and 0.05 Å. The grid points and the surface of Colavecchia *et al.*[40] are also shown for comparison. The value of ϵ used here is large in comparison with previous applications[54,55,56,57] and produces a root-mean-square error of 9.72 cm^{-1}. The *relative* error was larger than 1% at 67 geometries, 21 of which lie below the 3-body dissociation limit and are enclosed by 0.5 contour of the switching function (see Eq. (7) below). There are only 5 geometries at which the relative error is larger than 10%, and these lie either near the conical intersection or near the zero of the potential (where the relative error does not reflect the accuracy).

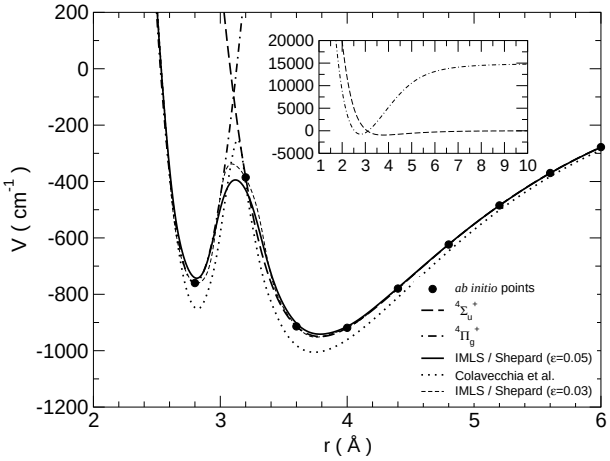

FIG. 5: Comparison of different fitted potentials with the *ab initio* energies for the quartet ground state of Li_3 at $D_{\infty h}$ geometries.

4. The long-range potential

The long-range potential, $V_{\rm LR}(\mathbf{r})$, was constructed as a sum of pairwise potentials and a nonadditive part as in Eq. (3). The need to include the nonadditive term has been described in detail in ref. 53. In particular, the sum of pair potentials gives an *isotropic* atom-diatom C_6 coefficient, whereas in reality there are important anisotropic terms. For the pairwise potentials $V_{\rm dimer}(r)$ we used the Li_2 RKR potential of Linton *et al.*,[50] which extrapolates to a three-term dispersion expression with coefficients C_6, C_8 and C_{10} as given by Yan *et al.*[49] The nonadditive potential was constructed as described in ref.[53] from the Axilrod-Teller-Muto triple-dipole term,[58,59] the third-order dipole-dipole-quadrupole dispersion energy,[60,61] the fourth-order dipole dispersion energy,[62,63] and an atom-diatom term that is short-range in one of the three distances,[53]

$$\begin{aligned} V_{3,\rm rep}(\mathbf{r}) = & - [A + BP_2(\cos\theta)] \exp(-Cx) r_{23}^{-3} r_{31}^{-3} \\ & \times [D_6(r_{23}) D_6(r_{31})]^{1/2} \\ & + \text{cyclic permutations}, \end{aligned} \tag{5}$$

where $x = (r_{12} - r_0)/r_0$ and θ is a Jacobi angle approximated in terms of internal angles φ_i as

$$P_2(\cos\theta) \simeq -\frac{1}{2}(1 + 3\cos\varphi_1 \cos\varphi_2 \cos\varphi_3). \tag{6}$$

All the non-additive terms were damped with a combination of Tang-Toennies damping functions D_6 and D_8[64] as described in ref. 53. Three-body dispersion coefficients Z_{111} and Z_{112} were taken from refs. 43 and 65, respectively, Z_{1111} was estimated as described in ref. 53, and the parameters A, B and C were determined as described in ref.[53] by fitting to the isotropic and anisotropic dispersion coefficients for Li + $Li_2(^3\Sigma_u^+)$ obtained as a function of r by Rérat *et al.*[66]

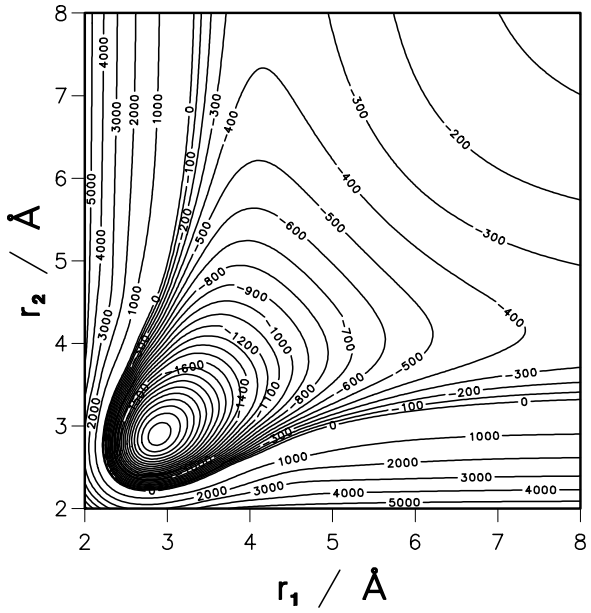

FIG. 6: The fitted quartet ground-state potential of lithium trimer for a bond angle of 60°. Contours are labeled in cm^{-1}.

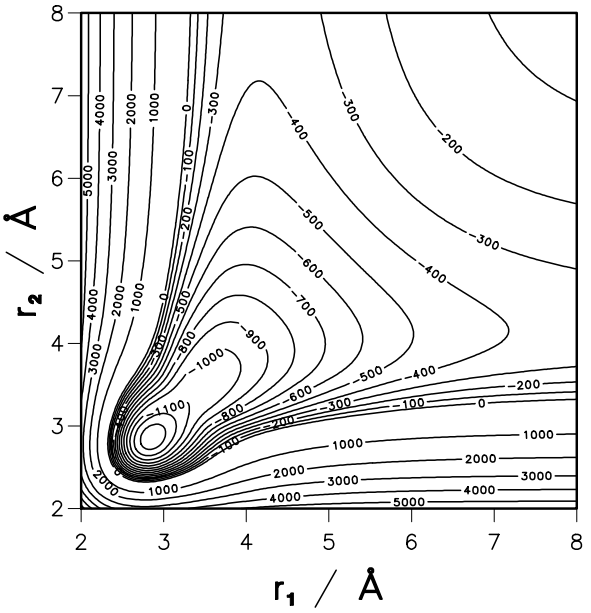

FIG. 7: The fitted quartet ground-state potential of lithium trimer for a bond angle of 120°. Contours are labeled in cm^{-1}.

The long-range form $V_{\rm LR}(\mathbf{r})$ is designed to be valid when *any* of the atom-atom distances is large. The short-range (IMLS) and long-range potentials were joined using the switching function

$$S(\mathbf{r}) = \frac{1}{2}\tanh[1 - s_1(r_{12} + r_{21} + r_{31} - s_2)], \qquad (7)$$

with s_1 set to 0.7 $Å^{-1}$ and s_2 to 20 Å.

Contour plots of the final potential for three different interbond angles α are shown in Figures 6 to 8.

III. LI + LI_2 SCATTERING CALCULATIONS

A. Methodology

Both linear and equilateral configurations of the Li_3 collision complex (and all geometries in between) lie lower in energy than Li + Li_2. The potential energy surface thus allows barrierless atom exchange (rearrangement) collisions even at limitingly low collision energies. Calculations using an inelastic formalism (including only one arrangement channel) are therefore inadequate. Accordingly, we have carried out quantum reactive scattering calculations to obtain collision cross sections. The methodology has been described in our previous work on ultracold collisions in Na + Na_2[20,21] and K + K_2[24] and also in studies of insertion reactions such as $N(^2D) + H_2 \rightarrow NH + H$,[67] $O(^1D) + H_2 \rightarrow OH + H$[68,69] and $S(^2D) + H_2 \rightarrow SH + H$[70] at thermal energies.

The time-independent Schrödinger equation is solved using a coupled-channel method in body-fixed democratic hyperspherical coordinates[71] using a diabatic-by-sector method. In each sector, the wavefunction is expanded in the eigenstates of a reference hamiltonian at a fixed hyperradius. The reference hamiltonian includes potential energy terms and kinetic energy terms arising from deformation and rotation around the axis of least moment of inertia. Its eigenfunctions are obtained by variational expansion in a set of pseudohyperspherical harmonics. The resulting coupled equa-

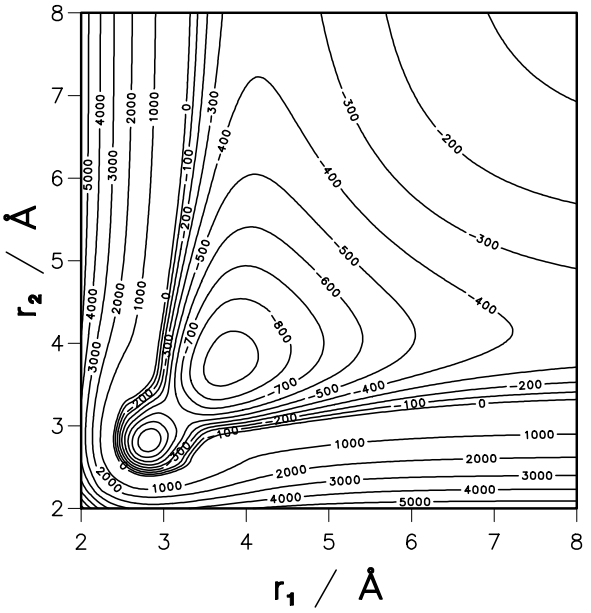

FIG. 8: The fitted quartet ground-state potential of lithium trimer for a bond angle of 150°. Contours are labeled in cm^{-1}.

tions are integrated using the log-derivative method of Manolopoulos.[72] At the point where interchannel couplings are small enough to be neglected, the coupled-channel solutions are matched onto atom-diatom functions propagated inwards in Jacobi coordinates to take account of the isotropic long-range and centrifugal potentials.

The diatom wavefunctions for Hund's case (b), which is appropriate for Li_2 ($^3\Sigma_u^+$), are labeled with a vibrational quantum number v and a mechanical rotational quantum number n; n couples with the diatomic electron spin $s = 1$ to give a resultant j. However, for Li_2 the splitting between states of the same n but different j are very small. We therefore do not introduce the spin explicitly and n and j are equivalent in our calculations.

The matching procedure yields the reactance matrix K, the scattering matrix S and the transition matrix $T = I - S$, where I is a unit matrix. The differential cross sections, averaged over initial m_n and summed over final m'_n states, are given by

$$\left(\frac{\mathrm{d}\sigma}{\mathrm{d}\Omega}\right)_{\tau vn\to\tau' v' n'} = \frac{1}{4(2n+1)k^2_{\tau vn}} \left|\sum_{JKK'} (2J+1) T^J_{\tau' v' n' K' \tau vnK} d^J_{KK'}(\vartheta)\right|^2, \tag{8}$$

where τ labels the arrangement, v and n indicate the vibrational and rotational quantum numbers of the diatom, K labels the z component of J and n in the body-fixed frame, and $k_{\tau vn}$ is the corresponding wave vector. Ω is an element of solid angle at a scattering angle ϑ with respect to the initial approach direction in the centre-of-mass frame and the d functions are reduced Wigner rotation matrices.

Integral state-to-state cross sections are obtained by integrating Eq. 8,

$$\sigma_{\tau vn\to\tau' v' n'} = \frac{\pi}{(2n+1)k^2_{\tau vn}} \sum_{JKK'} (2J+1) \left|T^J_{\tau' v' n' K' \tau vnK}\right|^2. \tag{9}$$

At ultralow energies, only T_{ii} matrix elements with atom-diatom end-over-end angular momentum $l = 0$ contribute significantly to the cross sections. The elastic and total inelastic cross sections in terms of T_{ii} are then

$$\sigma_{\mathrm{elas}} = \frac{\pi}{k^2}|T_{ii}|^2, \tag{10}$$

$$\sigma^{\mathrm{tot}}_{\mathrm{inel}} = \frac{\pi}{k^2}\left[1 - |1 - T_{ii}|^2\right], \tag{11}$$

where the τvn subscript has been dropped to simplify notation. At low energy, S_{ii} and T_{ii} are conveniently parameterized in terms of an energy-dependent complex scattering length $a(k) = \alpha(k) - \mathrm{i}\beta(k)$, where

$$a(k) = \frac{1}{\mathrm{i}k}\left(\frac{1 - S_{ii}}{1 + S_{ii}}\right) = \frac{1}{\mathrm{i}k}\left(\frac{T_{ii}}{2 - T_{ii}}\right). \tag{12}$$

The cross sections can be written exactly in terms of the energy-dependent scattering length,

$$\sigma_{\mathrm{elas}} = \frac{4\pi|a|^2}{1 + k^2|a|^2 + 2k\beta}, \tag{13}$$

$$\sigma^{\mathrm{tot}}_{\mathrm{inel}} = \frac{4\pi\beta}{k(1 + k^2|a|^2 + 2k\beta)}. \tag{14}$$

The scattering length becomes constant at limitingly low energy. If $ka \ll 1$, which is true at limitingly low energy except near a zero-energy resonance, Eq. 12 reduces to the expression commonly used for the zero-energy scattering length,[73]

$$a = \frac{1}{2\mathrm{i}} \lim_{k\to 0} \frac{T_{ii}}{k}. \tag{15}$$

Elastic and inelastic cross sections at ultralow energies are governed by the Wigner threshold laws,[74]

$$\sigma_{\mathrm{elas}} \sim E^{2l}, \qquad \sigma_{\mathrm{inel}} \sim E^{l-1/2}, \tag{16}$$

where E is the collision energy and l is the end-over-end angular momentum. In the presence of a long-range potential $-C_s r^{-s}$, elastic cross sections have an additional term $\sim E^{s-3}$ that dominates for higher l at ultralow energies.

B. Computational details

We have performed coupled-channel calculations on all possible mixtures of the two isotopes of lithium, ^{7}Li and ^{6}Li. The ^{7}Li nucleus is a fermion with nuclear spin 3/2, so that the atom, including its electrons, behaves as a composite boson in cold dilute gases. The ^{6}Li nucleus is a boson with nuclear spin 1, while the atom is a composite fermion. The present calculations are restricted to collisions in which all three of the atoms are in spin-stretched states (with $F = I + S = F_{\max}$ and $|M_F| = F$). For these states the nuclear spin wavefunction is symmetric with respect to any exchange of nuclei. However, the electronic wavefunction for the quartet state, which depends parametrically on nuclear coordinates, is antisymmetric with respect to exchange of two identical nuclei. This means that the spatial nuclear wavefunction must be symmetric under exchange of any two fermionic nuclei (bosonic alkali metal atoms) and antisymmetric under exchange of any two bosonic nuclei (fermionic alkali metal atoms). The symmetry under exchange of identical nuclei is easy to impose in our program by selecting pseudohyperspherical harmonics of appropriate symmetry in the basis set.

Propagation of the coupled-channel solutions is performed separately for each partial wave J^Π, labeled by the spin-free total angular momentum J, and parity eigenvalue Π. The parity is $(-1)^{n+l}$, and only l values

that satisfy the triangle inequality, $|J-n| \le l \le J+n$, are permitted.

The basis set for $^7Li_3$ included all eigenstates of the reference hamiltonian (see above) that match onto $^7Li_2$ states below the $v = 7$ manifold. Only even values of n are allowed for $^7Li_2$ in spin-stretched states. The resulting number of coupled equations varied between 97, for total angular momentum $J = 0$, and 827, for $J = 10$. For the $^6Li_3$ system, including only odd-n states of $^6Li_2$ below the $v = 7$ manifold gave a basis set that varied in size between 85 for $J = 0$ and 782 for $J = 11^-$. For $^6Li^7Li_2$ and $^7Li^6Li_2$, where the symmetry is reduced, the basis set even for $J = 0$ consisted of 272 and 263 functions, respectively. The calculation of eigenstates of the reference hamiltonian involved diagonalizations of matrices of sizes between 1240 and 2136 for $^7Li_3$, between 1220 and 2162 for $^6Li_3$, and between 3660 and 6488 for the isotopically mixed systems.

The coupled equations were integrated across a range of hyperradius ρ between 5 a_0 and 45 a_0 with a log-derivative sector width of 0.1 a_0. Within each sector, the wavefunction is propagated using the log-derivative method of Manolopoulos,[72] with a step size keyed to the local de Broglie wavelength. The propagation in the outer region in Jacobi coordinates extended as far as $R = 10000$ a_0 for collision energies of $E = 1$ nK.

C. Ultracold collisions

In the ultracold regime, the dominant contribution to cross sections comes from the partial wave that includes the $l = 0$ channel (s-wave scattering). For a particular initial rovibrational state (v, n), the cross section is thus calculated from the partial wave labeled by the total angular momentum $J = n$ and parity $\Pi = (-1)^n$. Figures 9 and 10 show the $J = 0$ cross sections for $^7Li + {}^7Li_2$ for initial states $(v, n) = (0, 0)$ and $(1, 0)$. The insets show the real and imaginary part of the complex scattering length, calculated using Eq. (12).

The energy dependence is particularly simple for collisions involving a ground-state $^7Li_2$ molecule, $(v, n) = (0, 0)$. Only elastic scattering is allowed below 2.3 K (the energy of the $(0, 2)$ threshold). The elastic cross sections are essentially constant below $\sim 10^{-5}$ K, and oscillate at higher energies. They exhibit sudden drops to zero at 37 mK and 300 mK and a feature around 750 mK. The one-channel scattering is characterized by a phase shift δ that can be extracted from the 1×1 K matrix element, $K_{11} = \tan\delta$.[75] The energy dependence of the phase shift is shown in Figure 11, and the zeroes in the cross section can be associated with δ passing through a multiple of π. The profile of the cross section follows $\sim \sin^2\delta$ and the associated minima are sometimes known as Ramsauer-Townsend minima.

The feature at $\sim$ 750 mK is different. It is associated with a sharp rise in δ through π, superimposed on the falling background. This is characteristic of a scattering resonance, and in this case is due to a Feshbach resonance involving a quasibound state associated with a rotationally excited threshold.

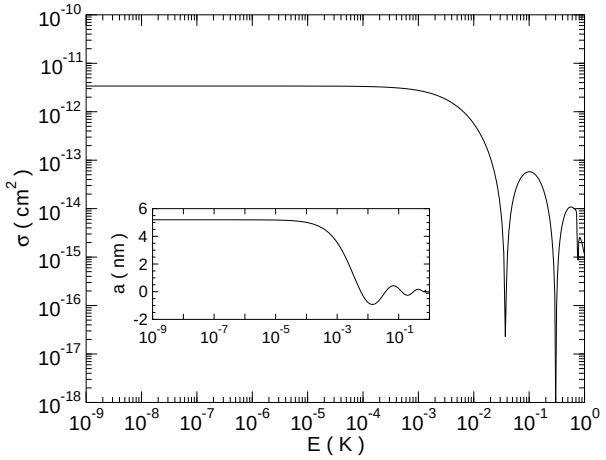

FIG. 9: Energy dependence of elastic cross sections for $^7Li + {}^7Li_2(v_i = 0, n_i = 0)$. The energy-dependent scattering length is shown in the inset.

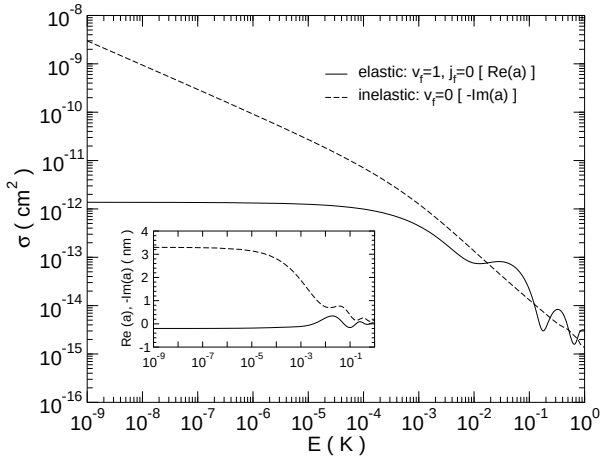

FIG. 10: Energy dependence of elastic and inelastic cross sections for $^7Li + {}^7Li_2(v_i = 1, n_i = 0)$. The complex energy-dependent scattering length is shown in the inset.

For the vibrationally excited initial state $(v, n) = (1, 0)$ the above arguments generalize. The S-matrix is now an 9×9 matrix with 8 inelastic (or reactive) channels corresponding to $v = 0$, $n = 0, 2, \ldots 14$. The elastic cross sections, Figure 12, still show oscillations, but these do not reach zero because the elastic S-matrix element cannot be 1 in the presence of inelastic scattering. The quantity that now shows a rise of π across a resonance is the eigenphase sum, which is the sum of phases obtained from eigenvalues of the K (or S) matrix. The eigenphase sum and the individual eigenphases are shown in Figure 13. It may be seen that there are two broad resonances centered at about 0.5 K and 0.8 K, but that the phase change associated with them is spread between all the

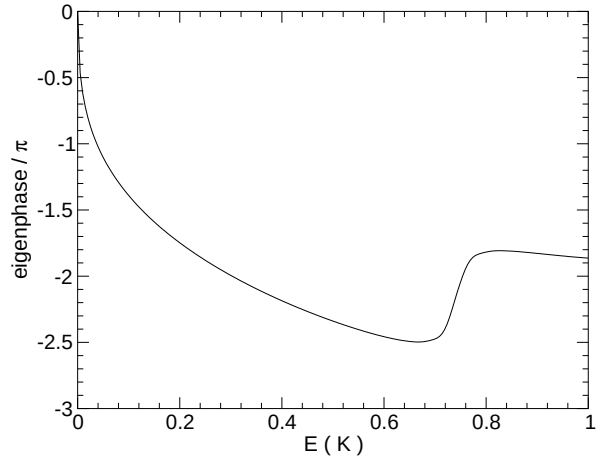

FIG. 11: Energy dependence of the phase shift δ for $^7\mathrm{Li} + {}^7\mathrm{Li}_2(v_i = 0, n_i = 0)$.

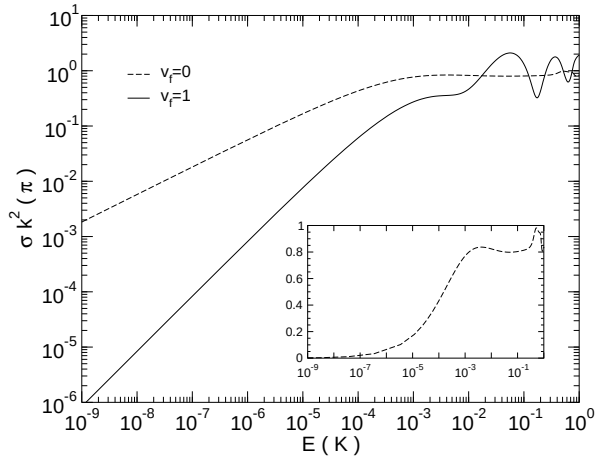

FIG. 12: Energy dependence of elastic and sum of inelastic probabilities, $\sigma k^2/\pi$, for $^7\mathrm{Li} + {}^7\mathrm{Li}_2(v_i = 1, n_i = 0)$.

channels. The individual eigenphases show a complicated pattern with many avoided crossings.

The inelastic cross sections show a slope of $-1/2$ on a log-log scale at ultralow temperatures, as predicted by the Wigner threshold law, Eq. (16). Above about 10^{-2} K, the slope changes to -1. The total inelastic probability, shown in Figure 12, increases with collision energy according to the Wigner laws and saturates close to unity outside the Wigner region.[20] At this point the energy dependence of the cross sections is governed by the kinematic prefactor $1/k^2$ in Eq. (11). A high inelastic probability is a feature of reactions proceeding over a deep well.[20,24,67,68,69,70]

The final state rotational distributions at ~ 1 nK are shown in Figure 14. The oscillatory structure is similar to that found earlier in ultracold collisions of Na + Na_2[20] and similar structures have been observed in vibrational predissociation of Van der Waals complexes. The

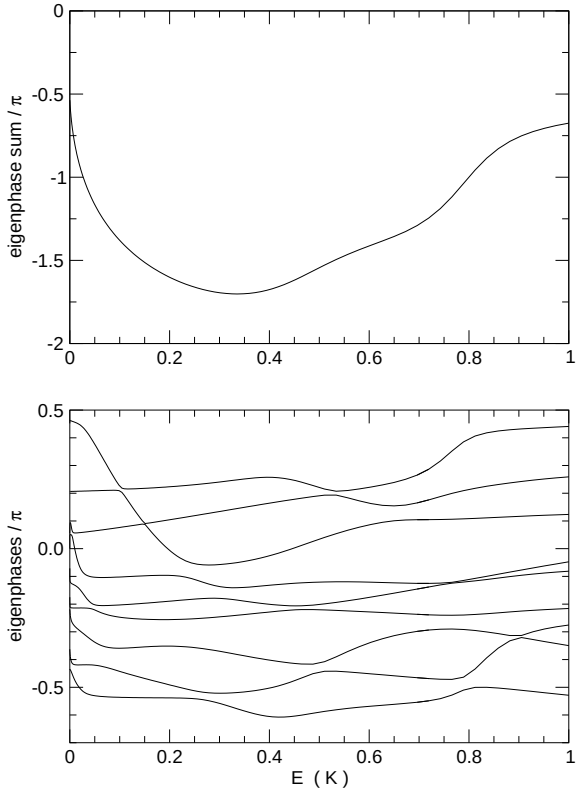

FIG. 13: Eigenphase sum (upper panel) and individual eigenphases (lower panel) for $^7\mathrm{Li} + {}^7\mathrm{Li}_2(v_i = 1, n_i = 0)$.

oscillation is thought to be due to a rotational rainbow effect.[76] In classical terms, the angular momentum imparted to the Li_2 molecule is zero if the kinetic energy is released at linear or T-shaped geometries, but large at around $\theta = 45°$. In this model, the oscillations arise from interference between classical trajectories on either side of the maximum.

The relative rotational distributions do not change significantly across the Wigner regime, although individual cross sections vary over five orders of magnitude between 1 nK and 100 mK because of the k^{-1} dependence of the Wigner threshold laws.

We have studied collisions involving a range of different initial molecular states. Results at a collision energy of ~ 1 nK are presented in Table II. There is no *systematic* dependence of the cross sections on the initial molecular state. Instead, the cross sections show essentially random scatter about a mean value. The origin of this behavior is discussed below. At 1 nK, the inelastic cross sections are typically three orders of magnitude higher than the elastic cross sections. The ratio decreases with the collision energy according to the Wigner laws, Eq. (16), until it reaches ~ 1 in the millikelvin range. Sympathetic and evaporative cooling of atoms and molecules depend on a low value ($< 10^{-2}$) of this ratio, so it is unlikely that such cooling mechanisms will be possible for alkali metal dimers in low-lying vibrationally excited states.

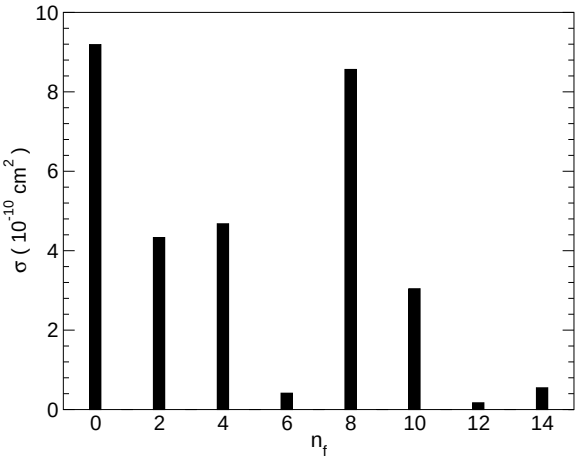

FIG. 14: Final rotational distributions for ^{7}Li + ^{7}Li$_2$(v_i = 1, $n_i = 0$) at 0.928 nK.

It has previously been found that collisions involving rotationally excited diatoms can cause unusually efficient and specific energy transfer when the collision time is longer than the rotational period.[77,78] This has been explained in terms of adiabatic invariance theory[79] with the assumption that the coupling between the degrees of freedom is not strong. This quasiresonant behaviour has also been studied at ultralow temperatures.[80,81,82,83] Inelastic transitions in some highly excited rotational levels of hydrogen molecules were found to be dramatically suppressed. We observe no evidence of such quasiresonant behaviour in Li + Li_2 collisions. Pure rotational transitions are as efficient as other rovibrational transitions in this strong-coupling case. The final-state rotational distributions tend to favor higher n levels for collisions of molecules in highly excited rotational levels, as in statistical models.

The atom-molecule inelastic loss rates observed in experiments on ultracold boson dimers ($^{133}Cs_2$),[14,19] are around 10^{-10} cm^3 s^{-1}, which is consistent with the cross sections obtained here for the bosonic lithium dimer ($^7Li_2$).

D. Cold collisions

At millikelvin collision energies, partial waves with end-over-end angular momentum $l > 0$ contribute significantly to the overall cross sections. The convergence of the elastic and inelastic probabilities $\sigma k^2/\pi$ with total angular momentum J is shown in Figures 15 and 16 for collisions with molecules in the $(1, 0)$ initial state. Partial waves $J = 0$ to 10 suffice to converge cross sections up to $\sim$ 580 mK, where the contribution of $J = 10$ to elastic and inelastic cross sections is 2.35% and 0.0655%, respectively. It may be seen that, for each energy, the inelastic cross sections are close to 1 for partial waves up to an energy-dependent cutoff value. The corresponding elastic cross sections oscillate around 1 until the cutoff is reached. Above 100 mK, convergence is slower for elastic probabilities, while below that it is slower for inelastic probabilities.

v_i, n_i	$\sigma_{\rm elas}$ (cm^2)	$\sigma_{\rm inel}$ (cm^2)	$\sigma_{\rm inel}/\sigma_{\rm elas}$
0, 0	3.39×10^{-12}	–	–
0, 2	4.87×10^{-12}	6.56×10^{-10}	135
0, 4	3.90×10^{-13}	9.55×10^{-10}	2450
0, 6	7.72×10^{-13}	9.42×10^{-10}	1220
0, 8	1.57×10^{-12}	2.04×10^{-9}	1300
0, 10	9.26×10^{-13}	2.55×10^{-9}	2750
1, 0	1.37×10^{-12}	3.09×10^{-9}	2260
1, 2	2.05×10^{-12}	3.00×10^{-9}	1460
1, 4	8.00×10^{-13}	1.14×10^{-9}	1425
1, 6	8.46×10^{-13}	1.43×10^{-9}	1690
1, 8	1.74×10^{-12}	1.96×10^{-9}	1130
1, 10	1.38×10^{-12}	1.53×10^{-9}	1110
2, 0	5.17×10^{-13}	4.77×10^{-10}	920
2, 2	1.02×10^{-12}	1.96×10^{-9}	1920
2, 4	1.25×10^{-12}	1.56×10^{-9}	1250
2, 6	8.83×10^{-13}	1.48×10^{-9}	1680
2, 8	9.85×10^{-13}	1.87×10^{-9}	1900
2, 10	1.32×10^{-12}	1.95×10^{-9}	1480
3, 0	9.29×10^{-13}	8.57×10^{-10}	920
3, 2	1.06×10^{-12}	1.43×10^{-9}	1350
3, 4	1.16×10^{-12}	2.42×10^{-9}	2090
3, 6	1.77×10^{-12}	2.61×10^{-9}	1470
3, 8	2.55×10^{-12}	3.85×10^{-9}	1510
3, 10	1.27×10^{-12}	1.96×10^{-9}	1540

TABLE II: Elastic and total inelastic cross sections and rate coefficients for ^{7}Li + ^{7}Li$_2$(v_i, n_i) at a collision energy of 0.928 nK for different initial states of the molecule.

The cross sections for partial waves with $J > 0$ also show a simple energy dependence. In the Wigner regime the inelastic cross sections increase with slope $l - 1/2$ on a log-log scale, with $l = J$ for $n_i = 0$. At energies above the centrifugal barrier they decrease with slope -1.

When several partial waves contribute significantly to the cross sections, the inelastic cross sections can be described semiquantitatively by classical Langevin capture theory. The assumption underlying this model is that the only condition for an inelastic event to take place is for the projectile to surmount the barrier of the effective potential resulting from the repulsive centrifugal and attractive long-range potential. For a long-range interaction of the form $-C_s/R^{-s}$ the effective potential is

$$V^l_{\rm eff}(R) = \frac{\hbar^2 l(l+1)}{2\mu R^2} - \frac{C_s}{R^s}. \qquad (17)$$

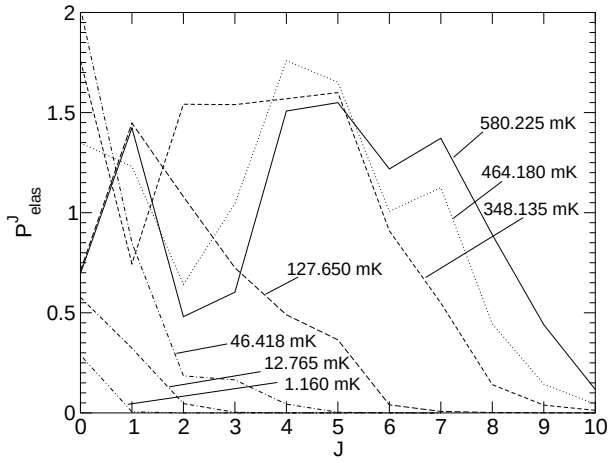

FIG. 15: Elastic probabilities, $\sigma k^2/\pi$, as a function of total angular momentum J for $^7\mathrm{Li} + {}^7\mathrm{Li}_2(v = 1, n = 0)$.

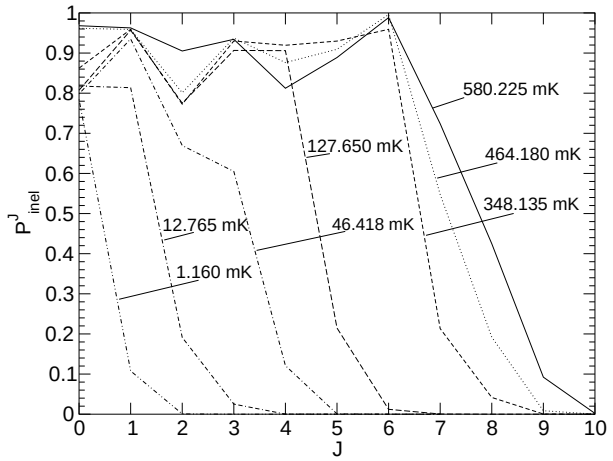

FIG. 16: Inelastic probabilities, $\sigma k^2/\pi$, as a function of total angular momentum J for $^7\mathrm{Li} + {}^7\mathrm{Li}_2(v = 1, n = 0)$.

This has a barrier height of

$$V^l_{\max} = \left[\frac{\hbar^2 l(l+1)}{\mu}\right]^{s/(s-2)} (sC_s)^{2/(2-s)} \left(\frac{1}{2} - \frac{1}{s}\right) \quad (18)$$

at an atom-diatom separation of

$$R^l_{\max} = \left(\frac{s\mu C_s}{\hbar^2 l(l+1)}\right)^{1/(s-2)} . \quad (19)$$

Taking $s = 6$, $C_6 = 3085.54\ E_h a_0^6$, and $\mu = 2m_{\mathrm{Li}}/3$, we obtain barrier heights of 2.78 mK, 14.4 mK, 40.8 mK, 87.9 mK, 161 mK for $l = 1$ to 5, at atom-molecule separations ranging from 94.25 a_0 for $l = 1$ to 47.89 a_0 for $l = 5$. At these distances the interaction is dominated by dispersion and is nearly isotropic. The Langevin expression for the inelastic cross section is

$$\sigma_{\mathrm{inel}}(E) = \frac{s\pi}{2}\left(\frac{2}{s-2}\right)^{(s-2)/s}\left(\frac{C_s}{E}\right)^{2/s} . \quad (20)$$

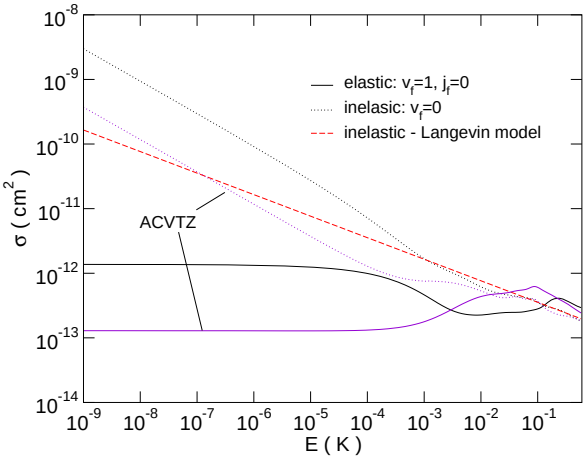

FIG. 17: [Color online] Elastic and total inelastic cross sections for $^7\mathrm{Li} + {}^7\mathrm{Li}_2(v_i = 1, n_i = 0)$ on the uncontracted cc-pV5Z and aug-cc-pCVTZ basis set potentials and the inelastic cross sections in the Langevin model.

The total inelastic cross sections are compared with this result in Figure 17 and it may be seen that there is increasingly good agreement between the full calculations and the Langevin model above about 30 mK.

To test that the agreement between the Langevin model and our results is not fortuitous, we recalculated the cross sections using partial waves $J = 0$ to 10 using a different potential surface, designated ACVTZ. The ACVTZ potential was obtained in the same manner as described above, but with electronic energies calculated using a considerably smaller basis set (aug-cc-pCVTZ). The potential is significantly different, with a global D_{3h} minimum 3873.37 cm^{-1} deep at $r = 3.125$ Å and a $D_{\infty h}$ minimum 930.29 cm^{-1} deep at $r = 3.780$ Å. The two potentials have the same long-range form, joined using the switching function of Eq. (7). The elastic and inelastic cross sections calculated using the ACVTZ potential are included in Figure 17. Once again the agreement with the Langevin model is excellent above ~ 30 mK, though the two potentials give cross sections that differ by about an order of magnitude in the Wigner regime. We found similar agreement with the model for collisions involving other initial molecular states. The Langevin cross sections are independent of the initial state, particle masses and the details of short-range potential.

Elastic cross sections are comparable to inelastic ones in the millikelvin region and can be as high as twice the inelastic ones. However, the ratio is never high enough to be favorable for the prospects of evaporative or sympathetic cooling. Whenever the Langevin model provides good estimates of inelastic cross sections, it implies that the inelastic probabilities are close to 1, which in turn implies that elastic cross sections (Eq. (10)) and inelastic cross sections (Eq. (11)) are not drastically different.

The reaction $^7\mathrm{Li} + {}^7\mathrm{Li}_2$ has no barrier for either linear or perpendicular approaches. The deep well in the

potential energy surface suggests that the reaction proceeds via an insertion mechanism involving complex formation. It is therefore interesting to compare the scattering results obtained here with those for insertion reactions that have been studied at ordinary temperatures ($\sim$ 100 meV).[67,68,69,70] These reactions are also characterized by high inelastic and reactive probabilities. The final-state vibrational distributions decrease with v and the rotational distributions peak at high n for each final v. If all product states are equally probable, the product state distribution is proportional to the density of available states, which depends on the rotational degeneracy and the density of translational states. The resulting differential cross sections display forward-backward symmetry. This can be explained by formation of a collision complex whose decay is statistical.[84] It has been shown that the exact quantum scattering results for insertion reactions are in excellent agreement with results based on a quantum statistical theory at thermal energies.[85]

The success of the Langevin model for total inelastic cross sections makes it worthwhile to investigate whether the product state distributions are well described by statistical theory. The statistical prior distributions are given by

$$p_{vn} \sim (2n+1)\sqrt{E - E_{vn}}, \tag{21}$$

where v and n refer to the final states and E is the total energy in the system.

Figure 18 compares the statistical predictions with full dynamics results in both the ultracold regime and at 580 mK for ^{7}Li + ^{7}Li$_2$ collisions for initial $(v, n) = (3, 0)$. The ultracold results are quite different from the statistical predictions and show oscillations with n for each v similar to those in Fig. 14. However, the oscillations start to wash out at higher energies and the rotational distributions start to resemble the statistical ones, though they still favor low rotational quantum numbers. The vibrational distributions are clearly some way from statistical even at 580 mK and favor high v (smaller changes in vibrational quantum number).

The corresponding results for differential cross sections are shown in Fig. 19. Statistical theory predicts forward-backward symmetry, but this has not fully developed even at 580 mK. Similar results have been obtained in the study of cold collisions of K + K$_2$.[24] The asymmetry probably arises from insufficient averaging over J in Eq. (8) at cold collision energies. We expect that at higher collision energies, where more partial waves contribute, the cross terms in Eq. (8) will vanish due to phase cancellations and the symmetry observed in other deep-well systems will be recovered.

E. Potential sensitivity

Cross sections for elastic atom-atom collisions in the limit of zero collision energy depend on a single parameter, the scattering length. The scattering length

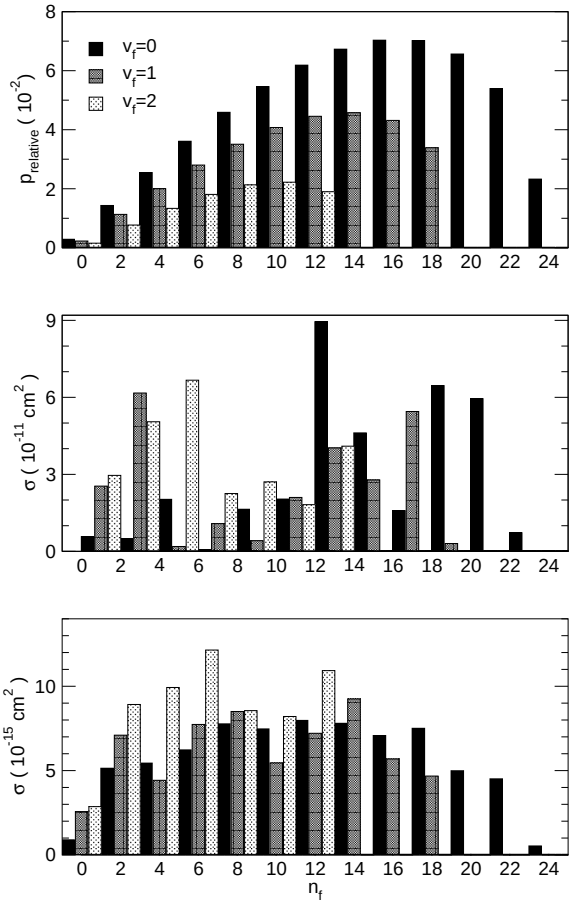

FIG. 18: Final rotational distributions for ^{7}Li + ^{7}Li$_2$($v_i = 3, n_i = 0$). Top panel: statistical prediction; center panel: ultracold regime (0.928 mK); bottom panel: collision energy of 580 mK.

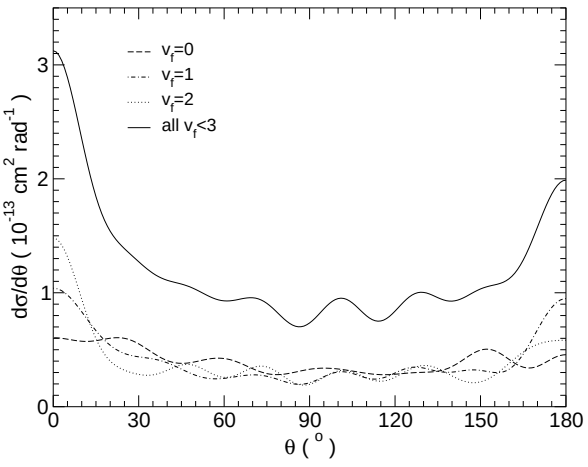

FIG. 19: Center-of-mass differential cross sections for ^{7}Li + ^{7}Li$_2$($v_i = 3, n_i = 0$) at a collision energy of 580 mK. Differential cross sections are integrated through the azimuthal angle and summed over the final states in each vibrational manifold.

is very sensitive to details of the interaction potential and its properties and dependence on potential are well established.[86] In particular, the scattering length passes through a pole whenever there is a bound state of the diatomic potential curve at exactly zero energy, and the elastic cross section shows a corresponding peak of height $4\pi/k^2$ (or $8\pi/k^2$ for identical bosons).

A quantitative theoretical prediction of the scattering length is within reach today only for the lightest diatomic systems and with the best available *ab initio* potentials.[87,88,89] For Li_2, the sensitivity of scattering length to small differences between potentials is illustrated in Table I. For heavier systems the variation of scattering length with potential parameters is usually too fast to allow quantitative predictions until experimental data are available to help determine the scattering length.

The absolute accuracy of the cross sections presented in this paper is limited by the quality of potential energy surface. The accuracy of the electronic energies is degraded by the limitations of the correlation treatment and the size of the basis set used. Moreover, the effects of conical intersections and the influence of the excited electronic state have been neglected in our calculations. It is thus very worthwhile to investigate how changes in the potential energy surface affect the ultracold scattering results.

Since the potential for Li_2 is accurately known, we modified the Li_3 potential by scaling the nonadditive part of the potential by a multiplicative parameter λ. The depth of the global minimum $V_{\rm min}$ varies with the scaling factor as $\Delta V_{\rm min}/\Delta\lambda \approx 5150$ cm^{-1} over the range studied.

The dependence of the elastic cross sections on the scaling factor λ for ^{7}Li + ^{7}Li$_2(v_i = 0, n_i = 0)$ at ~ 1 nK is shown in Figure 20. Whenever there is a bound state at exactly zero energy, the scattering length passes through a pole and the cross section shows a very high peak ($\sigma \approx 4\pi/k^2$). Near each pole is a point where $S_{ii} = 1$ so $\sigma = 0$. It may be seen that the cross section passes through about 10 cycles for a 1% change in λ.

The mean value of the cross section can be estimated using the formula for the mean scattering length $\overline{a}$ given by Gribakin and Flambaum.[86] Taking the isotropic atom-molecule dispersion coefficient $C_6 = 3085.54\ E_h a_0^6$, we obtain $\overline{a} = 5.83 \times 10^{-13}$ cm^2, which underestimates our accurate quantum results but gives the correct order of magnitude.

For collisions of molecules in vibrationally excited states $(v_i, n_i = 0)$ with $v_i = 1$ to 3, the dependence of elastic and inelastic cross sections at ~ 1 nK on λ is shown in Figures 21 and 22. The dependence is again oscillatory, but the frequency and amplitude of the oscillations are smaller for higher initial vibrational quantum numbers v_i. The elastic (inelastic) cross sections vary across the range by 186% (136%) for $v_i = 1$ and 64% (73%) for $v_i = 3$. The sharp peaks in cross sections associated with poles in scattering lengths are entirely washed out for higher values of v_i.

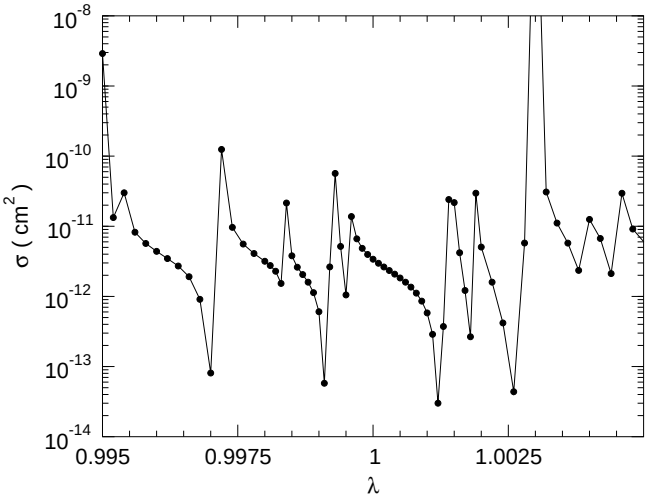

FIG. 20: Dependence of the elastic cross sections for ^{7}Li + ^{7}Li$_2(v_i = 0, n_i = 0)$ on the scaling factor λ of the nonadditive part of the potential.

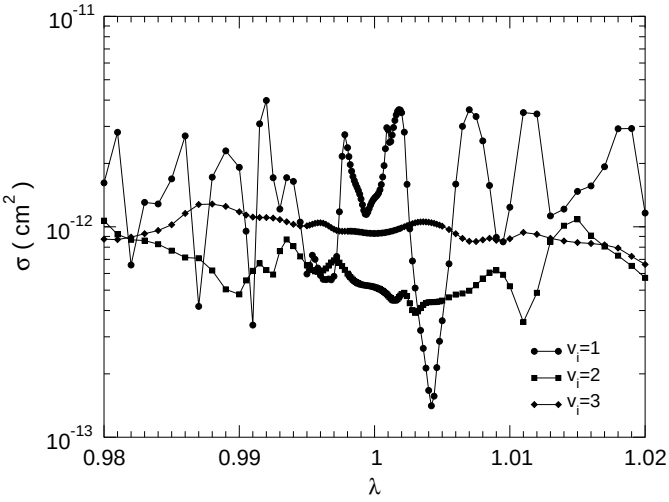

FIG. 21: Dependence of the elastic cross sections for ^{7}Li + ^{7}Li$_2(v_i, n_i = 0)$ on the scaling factor λ of the nonadditive part of the potential.

The lack of strong resonant peaks as a function of well depth for Li + Li_2 is an example of a general effect recently discussed by Hutson.[90] Similar effects have recently been observed when tuning through zero-energy Feshbach resonances in He + NH using magnetic fields.[91] In the presence of inelastic scattering, the complex scattering length $a = \alpha - i\beta$ exhibits an oscillation rather than a pole when a bound-state crosses threshold. The amplitude of the oscillation is characterized by a *resonant scattering length* $a_{\rm res}$. If the bound state is coupled with comparable strengths to the elastic and inelastic channels, the oscillation may be of relatively low amplitude and the peaks in cross sections are suppressed.

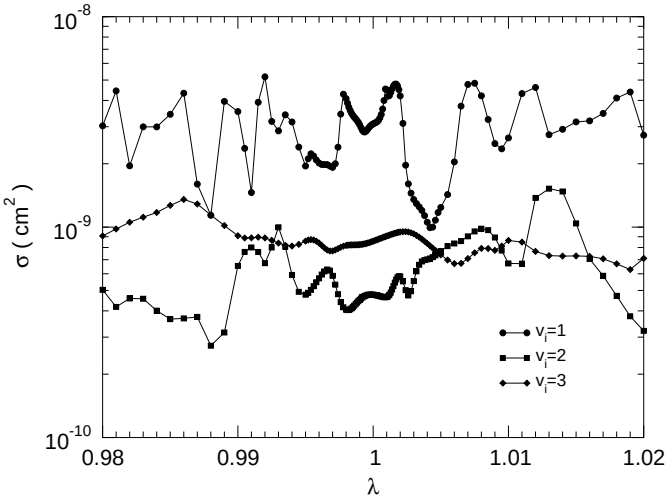

FIG. 22: Dependence of the total inelastic cross sections for ^{7}Li+^{7}Li$_2$($v_i, n_i = 0$) on the scaling factor λ of the nonadditive part of the potential.

This is the case in Li + Li_2, where there are strong couplings between all the channels involved. For $v_i = 1$ there is enough resonant coupling to the elastic channel that peaks are still observed, but even these have an amplitude of only about a factor of 10. For higher v_i, there are larger numbers of inelastic channels, each of which competes with the elastic channel and the resonant structures are progressively washed out.

The suppression of cross-section peaks observed here for Li + Li_2 contrasts with the situation commonly found for atom-atom scattering[3] and for atom-molecule reactive scattering in systems such as F + H_2.[92] For atom-atom collisions involving atoms in spin-stretched states, the resonant state is coupled to inelastic channels only by very week magnetic dipole-dipole interactions, but is coupled to the elastic channel by much stronger spin-exchange terms. This gives a large value of $a_{\rm res}$, corresponding to pole-like behavior of the scattering length and producing very large peaks in cross sections. Similarly, in F + H_2 the resonances studied[92] are due to quasibound states in the entrance channel, while the "inelastic" channels are actually reactive channels that are separated from the entrance well by a high barrier. This again gives very large peaks in cross sections. It is evident that the factor that suppresses the resonant peaks in Li + Li_2 is strong coupling to the inelastic channels.

A sensitivity study similar to the one we report here was performed on the Na + Na_2 system by Quéméner *et al.*[21] They also observed oscillations that decreased in amplitude with initial v.

F. Isotope effects

A strong suppression of inelastic rates has been observed experimentally in fermionic systems tuned to a large and positive atom-atom scattering length.[8,9,10,93] The molecular cloud consisting of weakly bound dimers of fermions exhibits remarkable stability against collisional decay. By contrast, the vibrational relaxation for weakly bound bosonic dimers is fast.[4,5,7,18,94] The suppression of inelastic scattering for fermionic systems has been interpreted in terms of the requirements of Fermi statistics.[22,23].

We have repeated all the above scattering calculations involving molecules in low-lying rovibrational states for the fermionic system ^{6}Li + ^{6}Li$_2$. A brief account of the results was given in ref. 25. For ^{6}Li + ^{6}Li$_2$, the dominant contribution to cross sections in the ultracold regime comes from total angular momentum $J = 1^-$, which is the partial wave that contains a contribution from $l_i = 0$. Cross sections at a collision energy of ≈ 1 nK are shown in Table III. The individual calculated values are significantly different from the bosonic case, but the effect is *not* due to suppression by Fermi statistics. Instead, the dominant effects is that the change in nuclear mass alters the scattering by a mechanism similar to a change in the potential surface, as discussed in the previous subsection. The cross sections calculated for individual initial states are thus once again scattered essentially randomly about a mean value. However, when we compare the results for a variety of initial rovibrational states, we see that there are no *systematic* differences between the overall rates for bosonic and fermionic systems for the low vibrational states that we have studied.

Unusually low inelastic rates (about an order of magnitude lower, with small Im(a)) were obtained for systems that have a small number of energetically accessible inelastic channels, such as ^{6}Li + ^{6}Li$_2$($v_i = 0, n_i = 3$) and ^{7}Li + ^{7}Li$_2$($v_i = 0, n_i = 2$).

The energy dependence of the cross sections in fermionic systems is qualitatively similar to that described above for bosonic systems. The Wigner regime is reached at energies around 10^{-5} K. For non-zero initial end-over-end angular momenta, the simple relationship of Eq. 16 holds at energies below the corresponding centrifugal barriers. At higher energies, the energy dependence of inelastic cross sections follows the Langevin model, Eq. 20.

For spin-stretched ^{6}Li + ^{6}Li$_2$ collisions, only odd rotational levels of Li_2 are allowed. Figure 23 shows the product rotational distribution for $v_i = 1$, $n_i = 1$ in the Wigner regime, and it may be seen that the distribution is again oscillatory. At higher collision energies the oscillations are washed out in the sum over partial waves, as shown in Figure 24. However, as for the bosonic system, the rotational distribution is significantly non-statistical. The forward-backward symmetry of the differential cross sections predicted by statistical theory is also not present for ^{6}Li + ^{6}Li$_2$ at 116 mK, as seen in Figure 25.

v_i, n_i	$\sigma_{\rm elas}$ (cm^2)	$\sigma_{\rm inel}$ (cm^2)	$\sigma_{\rm inel}/\sigma_{\rm elas}$
0, 1	2.20×10^{-12}	–	–
0, 3	1.11×10^{-12}	2.62×10^{-10}	236
0, 5	9.27×10^{-13}	2.17×10^{-9}	2340
0, 7	1.32×10^{-13}	8.90×10^{-10}	6740
0, 9	1.07×10^{-12}	1.81×10^{-9}	1690
0, 11	1.77×10^{-12}	2.37×10^{-9}	1340
1, 1	6.09×10^{-13}	1.40×10^{-9}	2300
1, 3	1.21×10^{-12}	1.21×10^{-9}	1000
1, 5	1.93×10^{-12}	2.59×10^{-9}	1340
1, 7	1.43×10^{-12}	2.02×10^{-9}	1410
1, 9	1.74×10^{-12}	1.96×10^{-9}	1130
1, 11	1.27×10^{-12}	2.31×10^{-9}	1820
2, 1	1.67×10^{-12}	2.26×10^{-9}	1350
2, 3	1.14×10^{-12}	2.23×10^{-9}	1960
2, 5	2.04×10^{-12}	2.80×10^{-9}	1370
2, 7	1.00×10^{-12}	2.52×10^{-9}	2520
2, 9	1.46×10^{-12}	3.20×10^{-9}	2190
2, 11	7.72×10^{-13}	1.77×10^{-9}	2290
3, 1	1.46×10^{-12}	2.76×10^{-9}	1890
3, 3	2.62×10^{-12}	2.57×10^{-9}	981
3, 5	1.87×10^{-12}	2.71×10^{-9}	1450
3, 7	1.31×10^{-12}	2.77×10^{-9}	2110
3, 9	1.17×10^{-12}	2.10×10^{-9}	1790
3, 11	6.92×10^{-13}	2.00×10^{-9}	2890

TABLE III: Elastic and total inelastic cross sections and rate coefficients for ^{6}Li + ^{6}Li$_2(v_i, n_i)$ at a collision energy of 0.928 nK for different initial states of the molecule.

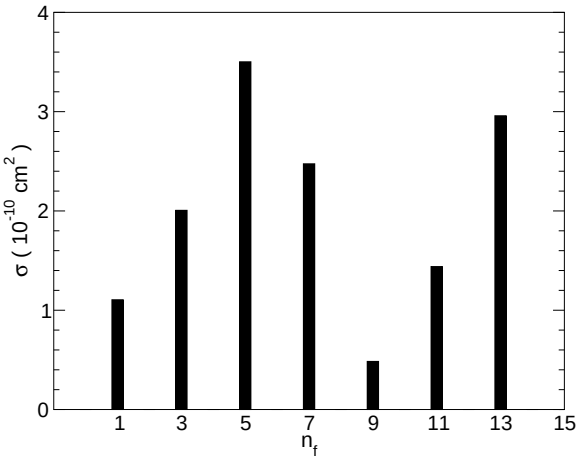

FIG. 23: Final rotational distributions for ^{6}Li + ^{6}Li$_2(v_i = 1, n_i = 1)$ at a collision energy in the Wigner regime.

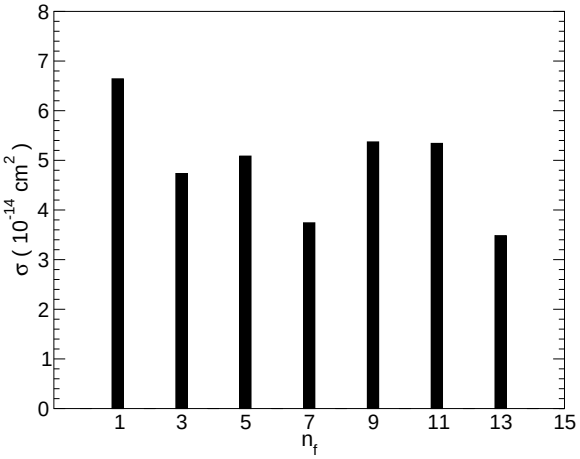

FIG. 24: Final rotational distributions for ^{6}Li + ^{6}Li$_2(v_i = 1, n_i = 1)$ at a collision energy of 116 mK.

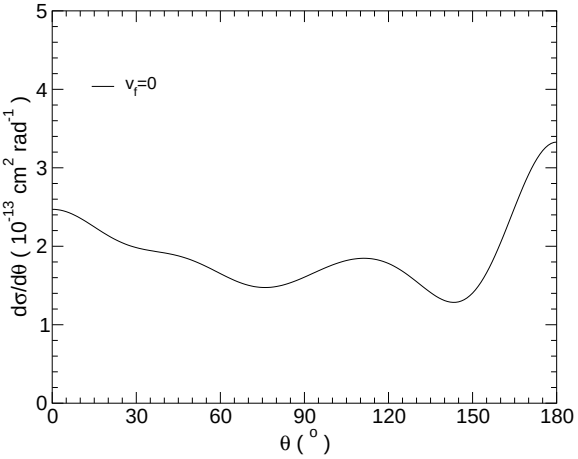

FIG. 25: Center-of-mass differential cross sections for ^{6}Li + ^{6}Li$_2(v_i = 1, n_i = 1)$ at a collision energy of 116 mK. Differential cross sections are integrated through the azimuthal angle and summed over the final states in each vibrational manifold and overall.

G. Reactions in isotopic mixtures

A greater variety of atom–diatom collisions may be observed in mixtures. Isotopic mixtures of ^{6}Li and ^{7}Li are of considerable interest,[95,96,97] and one can envisage creating either homonuclear or heteronuclear dimers in such a mixture. The atom-diatom collision systems of interest are

$$^7\mathrm{Li} + {}^6\mathrm{Li}^7\mathrm{Li}, \tag{22}$$

$$^7\mathrm{Li} + {}^6\mathrm{Li}_2. \tag{23}$$

$$^6\mathrm{Li} + {}^7\mathrm{Li}_2, \tag{24}$$

$$^6\mathrm{Li} + {}^6\mathrm{Li}^7\mathrm{Li}, \tag{25}$$

We have studied all four of the systems (22) to (25) and gave a preliminary report in ref. 26. The novel feature in these systems is the possibility of a chemical reaction in which the reactants and products are distinguishable. Because of the differences in zero-point energy, the reactions are exoergic even for ground-state molecules for the two systems involving atomic ^{7}Li, (22) and (23).

For ^{6}Li^{7}Li, both even and odd rotational levels are allowed even for spin-stretched states. The higher density of states makes these systems harder to treat computationally. Our calculations on these systems were therefore restricted to the $J = 0$ and 1 partial waves and are thus converged only at ultracold collision energies.

We will consider the systems that are reactive for ground-state molecules first. The cross sections, rate coefficients and scattering lengths for collisions of ^{7}Li with ^{6}Li^{7}Li in several different initial molecular states are summarized in Table IV. For molecules in excited vibrational or rotational states, the cross sections are comparable to those found for the homonuclear systems. However, for ^{6}Li^{7}Li($v = 0, n = 0$) the cross section for reaction is a factor of about 50 smaller than for other states. This corresponds to a reactive rate coefficient of 4.05×10^{-12} cm^3 s^{-1} and Im(a) = 0.233 Å. In this case there is only a single exoergic channel, with a kinetic energy release of 1.822 K. The small cross section is probably due to the small volume of available phase space for reaction.

The increased density of rotational states for ^{6}Li^{7}Li produces an increased density of Feshbach resonances. The energy-dependence of the eigenphase sum for ^{7}Li + ^{6}Li^{7}Li is shown in the top panel of Figure 26. There is a Feshbach resonance clearly visible at 225 mK and another at about 470 mK, though the latter overlaps the threshold for opening the $n = 2$ reactive channel at 477.2 mK. There are further overlapping resonances near 630 mK and 725 mK. The corresponding structures in the elastic and inelastic cross sections are shown in the lower two panels of Figure 26. The elastic cross section shows a Ramsauer-Townsend minimum near 120 mK. It dips to a very small value near the Feshbach resonance at 225 mK, but *not* near the resonance near 470 mK. The reactive cross section, by contrast, dips close to zero at *both* Feshbach resonances. This suggests the interesting possibility of reducing the inelastic/elastic cross section ratio by tuning close to a Feshbach resonance.

Reactive collisions of ^{7}Li with ^{6}Li$_2$ are more strongly exoergic because for spin-stretched states the ^{6}Li$_2$ molecule is restricted to odd rotational levels while the ^{6}Li^{7}Li molecule is not. Because of this collisions of ^{7}Li with ^{6}Li$_2$ in its $n = 1$ ground state can produce ^{6}Li^{7}Li in $n = 0$, 1 or 2. The calculated cross sections, rate coefficients and scattering lengths are summarized in Table V. The reactive cross sections for ^{6}Li$_2$ ($n = 1$) are again reduced compared to those for other states, but not as dramatically as for ^{7}Li + ^{6}Li^{7}Li ($n = 0$).

Ultracold collisions of ^{6}Li^{7}Li and ^{7}Li$_2$ with atomic ^{6}Li

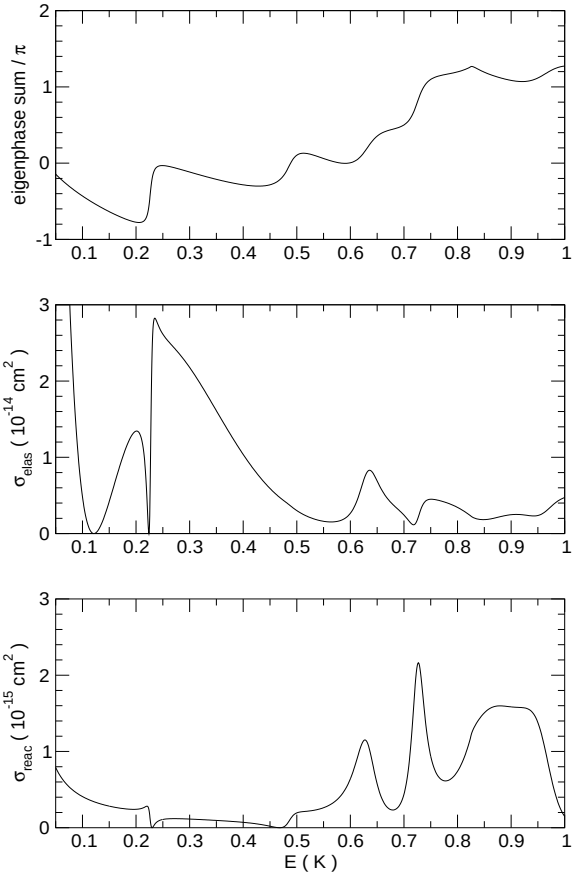

FIG. 26: Energy dependence of eigenphase sum (top panel), elastic cross section (center panel) and inelastic/reactive cross section (bottom panel) for collisions of ^{6}Li^{7}Li ($v = 0, n = 0$) with ^{7}Li.

are nonreactive unless the molecule is initially in a rovibrationally excited state. This is because for these systems the zero-point energy is greater in the products than in the reactants. The calculated cross sections, rate coefficients and scattering lengths for these systems are summarized in Tables VI and VII. The patterns of cross sections for rovibrationally excited initial states are fairly similar to those for the homonuclear systems, with no particularly small inelastic or reactive rates. The novel feature of these systems really lies in the fact that the reactions are forbidden for ground-state molecules, so that sympathetic cooling of molecules by contact with ^{6}Li atoms might be envisaged. For example, if ^{6}Li$_2$ molecules are produced in the presence of both ^{6}Li and ^{7}Li, they can react to form (relatively hot) ^{6}Li^{7}Li. If the ^{7}Li atoms are then removed, the molecules might be cooled by elastic collisions with ^{6}Li.

v_i, n_i	$\sigma_{\rm elas}$ (cm^2)	$\sigma_{\rm inel}$ (cm^2)	$\sigma_{\rm reac}$ (cm^2)	$k_{\rm loss}$ (cm^{3}s^{-1})	Re(a) (nm)	$-$Im(a) (nm)
0, 0	1.77×10^{-13}	–	2.20×10^{-11}	4.05×10^{-12}	1.19	0.0233
1, 0	1.32×10^{-12}	8.79×10^{-10}	2.56×10^{-10}	2.09×10^{-10}	3.01	1.19
2, 0	1.32×10^{-12}	1.37×10^{-9}	1.02×10^{-9}	4.40×10^{-10}	2.04	2.52
3, 0	1.09×10^{-12}	1.30×10^{-9}	8.74×10^{-10}	4.00×10^{-10}	1.86	2.29
0, 1	4.81×10^{-12}	4.30×10^{-10}	2.32×10^{-9}	5.06×10^{-10}	5.46	2.90
1, 1	1.52×10^{-12}	1.85×10^{-9}	9.47×10^{-10}	5.14×10^{-10}	1.85	2.94
2, 1	9.09×10^{-13}	1.22×10^{-9}	4.45×10^{-10}	2.93×10^{-10}	2.10	1.68
3, 1	9.51×10^{-13}	1.67×10^{-9}	6.28×10^{-10}	4.23×10^{-10}	1.71	2.15

TABLE IV: Cross sections and related parameters for ^{7}Li + ^{6}Li^{7}Li (v_i, n_i) at a collision energy of 0.928 nK for different initial states of the molecule.

v_i, n_i	$\sigma_{\rm elas}$ (cm^2)	$\sigma_{\rm inel}$ (cm^2)	$\sigma_{\rm reac}$ (cm^2)	$k_{\rm loss}$ (cm^{3}s^{-1})	Re(a) (nm)	$-$Im(a) (nm)
0, 1	1.17×10^{-12}		2.34×10^{-10}	4.37×10^{-11}	3.04	0.244
1, 1	1.62×10^{-12}	1.00×10^{-9}	1.76×10^{-9}	5.15×10^{-10}	2.17	2.86
2, 1	6.61×10^{-13}	2.66×10^{-10}	1.12×10^{-9}	2.58×10^{-10}	1.41	1.81
3, 1	8.05×10^{-13}	5.29×10^{-10}	1.07×10^{-9}	2.98×10^{-10}	1.91	1.66

TABLE V: Cross sections and related parameters for ^{7}Li + ^{6}Li$_2$ (v_i, n_i) at a collision energy of 0.928 nK for different initial states of the molecule.

v_i, n_i	$\sigma_{\rm elas}$ (cm^2)	$\sigma_{\rm inel}$ (cm^2)	$\sigma_{\rm reac}$ (cm^2)	$k_{\rm loss}$ (cm^{3}s^{-1})	Re(a) (nm)	$-$Im(a) (nm)
0, 0	4.71×10^{-12}				6.12	
1, 0	6.43×10^{-13}	1.15×10^{-9}	2.12×10^{-10}	2.64×10^{-10}	1.81	1.36
2, 0	1.12×10^{-12}	1.39×10^{-9}	4.37×10^{-10}	3.53×10^{-10}	2.36	1.82
3, 0	1.54×10^{-12}	1.34×10^{-9}	9.49×10^{-10}	4.43×10^{-10}	2.66	2.29
0, 1	2.74×10^{-12}	5.84×10^{-10}		1.13×10^{-10}	4.64	0.586
1, 1	7.56×10^{-13}	2.04×10^{-9}	2.72×10^{-10}	4.48×10^{-10}	0.828	2.31
2, 1	1.19×10^{-12}	2.07×10^{-9}	7.21×10^{-10}	5.40×10^{-10}	1.32	2.79
3, 1	1.27×10^{-12}	1.55×10^{-9}	7.76×10^{-10}	4.51×10^{-10}	2.16	2.33

TABLE VI: Cross sections and related parameters for ^{6}Li + ^{6}Li^{7}Li (v_i, n_i) at a collision energy of 0.928 nK for different initial states of the molecule.

v_i, n_i	$\sigma_{\rm elas}$ (cm^2)	$\sigma_{\rm inel}$ (cm^2)	$\sigma_{\rm reac}$ (cm^2)	$k_{\rm loss}$ (cm^{3}s^{-1})	Re(a) (nm)	$-$Im(a) (nm)
0, 0	1.29×10^{-12}				3.20	
1, 0	1.33×10^{-12}	5.70×10^{-10}	8.85×10^{-10}	2.79×10^{-10}	2.90	1.47
2, 0	1.14×10^{-12}	1.39×10^{-9}	1.37×10^{-9}	5.28×10^{-10}	1.16	2.79
3, 0	1.51×10^{-12}	1.00×10^{-9}	1.42×10^{-9}	4.63×10^{-10}	2.45	2.45

TABLE VII: Cross sections and related parameters for ^{6}Li + ^{7}Li$_2$ (v_i, n_i) at a collision energy of 0.928 nK for different initial states of the molecule.

IV. CONCLUSIONS

We have developed a new potential energy surface for quartet Li + Li_2 from high-level electronic structure calculations and used it to carry out quantum dynamics calculations on elastic, inelastic and reactive collisions on Li + Li_2 under cold and ultracold collisions. The potential energy surface was calculated using RCCSD(T) calculations with all electrons correlated. The surface was calculated on a grid in pure bond-length coordinates. It was interpolated at short range using the interpolant-moving least-squares method and merged with a long-range form that is correct at both the atom-diatom and the atom-atom-atom dissociation limits.

The potential energy surface has a deep triangular minimum that lies far below the atom-diatom energy and allows barrierless atom exchange reactions. The well depth is a factor of 4 deeper than would be expected on the basis of a pairwise-additive sum of triplet Li_2 potentials. The surface exhibits a seam of conical intersections at linear geometries, at energies close to that at three separated Li atoms.

Quantum dynamics calculations were carried out in a time-independent reactive scattering formalism based on an expansion in pseudohyperspherical harmonics. This approach makes it straightforward to include the required symmetry with respect to exchange of identical bosons (^{7}Li atoms) or fermions (^{6}Li atoms). For the homonuclear systems ^{7}Li + $^7Li_2$ and ^{6}Li + $^6Li_2$, the products of reactive and non-reactive collisions are indistinguishable. Nevertheless, all collisions involving vibrationally excited Li_2 result in very fast vibrational relaxation (quenching). For the low-lying vibrationally excited states studied here, there is *no* systematic suppression of quenching rates for collisions involving fermion dimers ($^6Li_2$). This contrasts with the situation found both experimentally and theoretically for fermion dimers produced by Feshbach resonance tuning in their highest vibrational state.

For collisions involving mixtures of Li isotopes, reactive and nonreactive collision outcomes can be distinguished. In particular, for collisions of ^{7}Li atoms with either $^6Li_2$ or ^{6}Li^{7}Li, exoergic reactive collisions are possible even for vanishing kinetic energy because of the difference in zero-point energy between reactants and products. These reactive processes are generally very fast, except for the case of ^{7}Li + ^{6}Li^{7}Li ($v = 0, n = 0$) at collision energies below 477 mK, for which there is only one reactive channel.

The Li + Li_2 collision systems have a rich structure of scattering resonances at low energies. These are principally rotational Feshbach resonances due to quasibound states that correlate with rotationally excited diatomic molecules. Tuning such Feshbach resonances with applied magnetic fields offers possibilities for *controlling* ultracold molecular collisions, and this will be a topic for future work.

We have investigated the sensitivity of elastic and inelastic cross sections to variations in the interaction potential. Such variations tune Feshbach resonances across thresholds, and our expectation was that the cross sections would show very large peaks when this occurred. This is indeed the case for collisions of ground-state molecules where only elastic scattering is possible. For such collisions the elastic cross sections increase by many orders of magnitude close to each resonance, and the density of states is such that a 1% change in the potential depth sweeps about 10 resonances across threshold. However, for collisions where inelastic scattering is also possible the resonant behavior is strongly suppressed. The amplitude of the oscillations in cross sections decreases dramatically with increasing initial vibrational quantum number, and for $v = 3$ the cross section changes by no more than a factor of 2 as resonances cross threshold. This shows that, in some cases, cross sections are much less sensitive to small variations in the potential than was previously expected.

Acknowledgments

MTC is grateful for sponsorship from the University of Durham and Universities UK.

[1] J. M. Hutson and P. Soldán, Int. Rev. Phys. Chem. **25**, 497 (2006).
[2] K. M. Jones, E. Tiesinga, P. D. Lett, and P. S. Julienne, Rev. Mod. Phys. **78**, 483 (2006).
[3] T. Köhler, K. Goral, and P. S. Julienne, Rev. Mod. Phys. **78**, 1311 (2006).
[4] E. A. Donley, N. R. Claussen, S. T. Thompson, and C. E. Wieman, Nature **417**, 529 (2002).
[5] J. Herbig, T. Kraemer, M. Mark, T. Weber, C. Chin, H. C. Nägerl, and R. Grimm, Science **301**, 1510 (2003).
[6] K. Xu, T. Mukaiyama, J. R. Abo-Shaeer, J. K. Chin, D. E. Miller, and W. Ketterle, Phys. Rev. Lett. **91**, 210402 (2003).
[7] S. Dürr, T. Volz, A. Marte, and G. Rempe, Phys. Rev. Lett. **92**, 020406 (2004).
[8] K. E. Strecker, G. B. Partridge, and R. G. Hulet, Phys. Rev. Lett. **91**, 080406 (2003).
[9] J. Cubizolles, T. Bourdel, S. J. J. M. F. Kokkelmans, G. V. Shlyapnikov, and C. Salomon, Phys. Rev. Lett. **91**, 240401 (2003).
[10] S. Jochim, M. Bartenstein, A. Altmeyer, G. Hendl, C. Chin, J. H. Denschlag, and R. Grimm, Phys. Rev. Lett. **91**, 240402 (2003).
[11] S. Jochim, M. Bartenstein, A. Altmeyer, G. Hendl, S. Riedl, C. Chin, J. H. Denschlag, and R. Grimm, Science **302**, 2101 (2003).
[12] M. W. Zwierlein, C. A. Stan, C. H. Schunck, S. M. F. Raupach, S. Gupta, Z. Hadzibabic, and W. Ketterle, Phys.

Rev. Lett. **91**, 250401 (2003).
[13] M. Greiner, C. A. Regal, and D. S. Jin, Nature **426**, 537 (2003).
[14] P. Staanum, S. D. Kraft, J. Lange, R. Wester, and M. Weidemüller, Phys. Rev. Lett. **96**, 023201 (2006).
[15] J. M. Sage, S. Sainis, T. Bergeman, and D. DeMille, Phys. Rev. Lett. **94**, 203001 (2005).
[16] J. M. Hutson and P. Soldán, Int. Rev. Phys. Chem. **26**, 1 (2007).
[17] R. Wynar, R. S. Freeland, D. J. Han, C. Ryu, and D. J. Heinzen, Science **287**, 1016 (2000).
[18] T. Mukaiyama, J. R. Abo-Shaeer, K. Xu, J. K. Chin, and W. Ketterle, Phys. Rev. Lett. **92**, 180402 (2004).
[19] N. Zahzam, T. Vogt, M. Mudrich, D. Comparat, and P. Pillet, Phys. Rev. Lett. **96**, 023202 (2006).
[20] P. Soldán, M. T. Cvitaš, J. M. Hutson, P. Honvault, and J. M. Launay, Phys. Rev. Lett. **89**, 153201 (2002).
[21] G. Quéméner, P. Honvault, and J. M. Launay, Eur. Phys. J. D **30**, 201 (2004).
[22] D. S. Petrov, C. Salomon, and G. V. Shlyapnikov, Phys. Rev. Lett. **93**, 090404 (2004).
[23] D. S. Petrov, C. Salomon, and G. V. Shlyapnikov, Phys. Rev. A **71**, 012708 (2005).
[24] G. Quéméner, P. Honvault, J. M. Launay, P. Soldán, D. E. Potter, and J. M. Hutson, Phys. Rev. A **71**, 032722 (2005).
[25] M. T. Cvitaš, P. Soldán, J. M. Hutson, P. Honvault, and J. M. Launay, Phys. Rev. Lett. **94**, 033201 (2005).
[26] M. T. Cvitaš, P. Soldán, J. M. Hutson, P. Honvault, and J. M. Launay, Phys. Rev. Lett. **94**, 200402 (2005).
[27] J. Higgins, T. Hollebeek, J. Reho, T. S. Ho, K. K. Lehmann, H. Rabitz, G. Scoles, and M. Gutowski, J. Chem. Phys. **112**, 5751 (2000).
[28] P. Soldán, M. T. Cvitaš, and J. M. Hutson, Phys. Rev. A **67**, 054702 (2003).
[29] D. A. Brue, X. Li, and G. A. Parker, J. Chem. Phys. **123**, 091101 (2005).
[30] H.-J. Werner and W. Meyer, J. Chem. Phys. **73**, 2342 (1980).
[31] H.-J. Werner and W. Meyer, J. Chem. Phys. **74**, 5794 (1981).
[32] H.-J. Werner and P. J. Knowles, J. Chem. Phys. **82**, 5053 (1985).
[33] P. J. Knowles and H.-J. Werner, Chem. Phys. Lett. **115**, 259 (1985).
[34] H.-J. Werner, Adv. Chem. Phys. **69**, 1 (1987).
[35] H.-J. Werner, P. J. Knowles, R. Lindh, M. Schütz, P. Celani, T. Korona, F. R. Manby, G. Rauhut, R. D. Amos, A. Bernhardsson, et al., *Molpro, version 2002.6, a package of ab initio programs* (2003), see http://www.molpro.net.
[36] *Emsl gaussian basis set order form at http://www.emsl.pnl.gov/forms/basisform.html*.
[37] H.-J. Werner and E. A. Reinsch, J. Chem. Phys. **76**, 3144 (1982).
[38] P. J. Knowles and H.-J. Werner, Chem. Phys. Lett. **145**, 514 (1988).
[39] H.-J. Werner and P. J. Knowles, J. Chem. Phys. **89**, 5803 (1988).
[40] F. D. Colavecchia, J. P. Burke, W. J. Stevens, M. R. Salazar, G. A. Parker, and R. T Pack, J. Chem. Phys. **118**, 5484 (2003).
[41] T. H. Dunning, Jr., J. Chem. Phys. **90**, 1007 (1989).
[42] M. A. Iron, M. Oren, and J. M. L. Martin, Mol. Phys. **101**, 1345 (2003).
[43] Z. C. Yan, J. F. Babb, A. Dalgarno, and G. W. F. Drake, Phys. Rev. A **54**, 2824 (1996).
[44] R. W. Molof, H. L. Schwartz, T. M. Miller, and B. Bederson, Phys. Rev. A **10**, 1131 (1974).
[45] C. E. Moore, *Atomic Energy Levels*, vol. 1 (National Bureau of Standards, Washington, 1971).
[46] S. F. Boys and F. Bernardi, Mol. Phys. **19**, 553 (1970).
[47] T. S. Ho and H. Rabitz, J. Chem. Phys. **104**, 2584 (1996).
[48] T. S. Ho and H. Rabitz, J. Chem. Phys. **113**, 3960 (2000).
[49] Z. C. Yan, A. Dalgarno, and J. F. Babb, Phys. Rev. A **55**, 2882 (1997).
[50] C. Linton, F. Martin, A. J. Ross, I. Russier, P. Crozet, A. Yiannopoulou, L. Li, and A. M. Lyyra, J. Mol. Spectrosc. **196**, 20 (1999).
[51] E. R. I. Abraham, W. I. McAlexander, C. A. Sackett, and R. G. Hulet, Phys. Rev. Lett. **74**, 1315 (1995).
[52] T. J. Lee and P. R. Taylor, Int. J. Quantum Chem. pp. 199–207 (1989).
[53] M. T. Cvitaš, P. Soldán, and J. M. Hutson, Mol. Phys. **104**, 23 (2006).
[54] T. Ishida and G. C. Schatz, J. Comput. Chem. **24**, 1077 (2003).
[55] T. Ishida and G. C. Schatz, J. Chem. Phys. **107**, 3558 (1997).
[56] T. Ishida and G. C. Schatz, Chem. Phys. Lett. **298**, 285 (1998).
[57] J. Ischtwan and M. A. Collins, J. Chem. Phys. **100**, 8080 (1994).
[58] B. M. Axilrod and E. Teller, J. Chem. Phys. **11**, 299 (1943).
[59] Y. Muto, Proc. Phys. Math. Soc. Japan **17**, 629 (1943).
[60] R. J. Bell, J. Phys. B – At. Mol. Opt. Phys. **3**, 751 (1970).
[61] M. B. Doran and I. J. Zucker, J. Phys. C – Solid St. Phys. **4**, 307 (1971).
[62] W. L. Bade, J. Chem. Phys. **27**, 1280 (1957).
[63] W. L. Bade, J. Chem. Phys. **28**, 282 (1958).
[64] K. T. Tang and J. P. Toennies, J. Chem. Phys. **80**, 3726 (1984).
[65] S. H. Patil and K. T. Tang, J. Chem. Phys. **106**, 2298 (1997).
[66] M. Rérat and B. Bussery-Honvault, Mol. Phys. **101**, 373 (2003).
[67] P. Honvault and J. M. Launay, J. Chem. Phys. **111**, 6665 (1999).
[68] P. Honvault and J. M. Launay, J. Chem. Phys. **114**, 1057 (2001).
[69] F. J. Aoiz, L. Banares, J. F. Castillo, M. Brouard, W. Denzer, C. Vallance, P. Honvault, J. M. Launay, A. J. Dobbyn, and P. J. Knowles, Phys. Rev. Lett. **86**, 1729 (2001).
[70] P. Honvault and J. M. Launay, Chem. Phys. Lett. **370**, 371 (2003).
[71] J. M. Launay and M. LeDourneuf, Chem. Phys. Lett. **163**, 178 (1989).
[72] D. E. Manolopoulos, J. Chem. Phys. **85**, 6425 (1986).
[73] N. Balakrishnan, V. Kharchenko, R. C. Forrey, and A. Dalgarno, Chem. Phys. Lett. **280**, 5 (1997).
[74] E. P. Wigner, **73**, 1002 (1948).
[75] C. J. Ashton, M. S. Child, and J. M. Hutson, J. Chem. Phys. **78**, 4025 (1983).
[76] J. M. Hutson, C. J. Ashton, and R. J. Le Roy, J. Phys. Chem. **87**, 2713 (1983).
[77] B. Stewart, P. D. Magill, T. P. Scott, J. Derouard, and D. E. Pritchard, Phys. Rev. Lett. **60**, 282 (1988).
[78] P. D. Magill, B. Stewart, N. Smith, and D. E. Pritchard,

Phys. Rev. Lett. **60**, 1943 (1988).
[79] W. J. Hoving and R. Parson, Chem. Phys. Lett. **158**, 222 (1989).
[80] R. C. Forrey, V. Kharchenko, N. Balakrishnan, and A. Dalgarno, Phys. Rev. A **59**, 2146 (1999).
[81] R. C. Forrey, Phys. Rev. A **66**, 023411 (2002).
[82] P. M. Florian, M. Hoster, and R. C. Forrey, Phys. Rev. A **70**, 032709 (2004).
[83] K. Tilford, M. Hoster, P. M. Florian, and R. C. Forrey, Phys. Rev. A **69**, 052705 (2004).
[84] R. D. Levine and R. B. Bernstein, *Molecular Reaction Dynamics and Chemical Reactivity* (Oxford University Press, 1987).
[85] E. J. Rackham, T. Gonzalez-Lezana, and D. E. Manolopoulos, J. Chem. Phys. **119**, 12895 (2003).
[86] G. F. Gribakin and V. V. Flambaum, Phys. Rev. A **48**, 546 (1993).
[87] F. X. Gadea, T. Leininger, and A. S. Dickinson, Eur. Phys. J. D **15**, 251 (2001).
[88] F. X. Gadea, T. Leininger, and A. S. Dickinson, J. Chem. Phys. **117**, 7122 (2002).
[89] A. S. Dickinson, F. X. Gadea, and T. Leininger, J. Phys. B – At. Mol. Opt. Phys. **37**, 587 (2004).
[90] J. M. Hutson, arXiv:physics/0610210 (2006).
[91] M. L. González-Martínez and J. M. Hutson, Phys. Rev. A p. 022702 (2007).
[92] E. Bodo, F. A. Gianturco, N. Balakrishnan, and A. Dalgarno, J. Phys. B – At. Mol. Opt. Phys. **37**, 3641 (2004).
[93] C. A. Regal, M. Greiner, and D. S. Jin, Phys. Rev. Lett. **92**, 083201 (2004).
[94] J. Stenger, S. Inouye, M. R. Andrews, H. J. Miesner, D. M. Stamper-Kurn, and W. Ketterle, Phys. Rev. Lett. **82**, 2422 (1999).
[95] A. G. Truscott, K. E. Strecker, W. I. McAlexander, G. B. Partridge, and R. G. Hulet, Science **291**, 2570 (2001).
[96] F. Schreck, G. Ferrari, K. L. Corwin, J. Cubizolles, L. Khaykovich, M. O. Mewes, and C. Salomon, Phys. Rev. A **6401**, 011402 (2001).
[97] L. Khaykovich, F. Schreck, J. Cubizolles, T. Bourdel, K. L. Corwin, G. Ferrari, and C. Salomon, Physica B **329**, 13 (2003).